European Journal of Medicinal Chemistry 179 (2019) 765–778

Contents lists available at ScienceDirect

European Journal of Medicinal Chemistry

journal homepage: http://www.elsevier.com/locate/ejmech

Research paper

Discovery and characterization of trypanocidal cysteine protease inhibitors from the 'malaria box'

Glaécia A.N. Pereira [a, b], Elany B. da Silva [a], Saulo F.P. Braga [a, b], Paulo Gaio Leite [c], Luan C. Martins [a], Rafael P. Vieira [a, b], Wai Tuck Soh [d], Filipe S. Villela [a], Francielly M.R. Costa [a], Debalina Ray [e], Saulo F. de Andrade [f], Hans Brandstetter [d], Renata B. Oliveira [g], Conor R. Caffrey [h], Fabiana S. Machado [c], Rafaela S. Ferreira [a, *]

[a] Laboratório de Modelagem Molecular e Planejamento de Fármacos, Departamento de Bioquímica e Imunologia, Universidade Federal de Minas Gerais, Avenida Antonio Carlos 6627, Belo Horizonte, MG, 31270-901, Brazil
[b] CAPES Foundation, Ministry of Education of Brazil, Brasília, DF, Brazil
[c] Departamento de Bioquímica e Imunologia, Universidade Federal de Minas Gerais, Avenida Antonio Carlos 6627, Belo Horizonte, MG, 31270-901, Brazil
[d] Structural Biology Group By Department of Biosciences, University of Salzburg, Salzburg, Austria
[e] University of California San Francisco, 1700 4th Street, San Francisco, CA, 94158, USA
[f] Pharmaceutical Synthesis Group (PHARSG), Universidade Federal Do Rio Grande Do Sul, Porto Alegre, RS, Brazil
[g] Faculdade de Farmácia, Universidade Federal de Minas Gerais, Avenida Antonio Carlos 6627, Belo Horizonte, MG, 31270-901, Brazil
[h] Center for Discovery and Innovation in Parasitic Diseases, Skaggs School of Pharmacy and Pharmaceutical Sciences, University of California San Diego, 9500 Gilman Drive, La Jolla, CA, 92093, USA

ARTICLE INFO

Article history:
Received 6 May 2019
Received in revised form
19 June 2019
Accepted 21 June 2019
Available online 22 June 2019

Keywords:
Malaria box
Small molecules
Cysteine protease inhibitors
Rhodesain
Cruzain
SmCB1

ABSTRACT

Chagas disease, Human African Trypanosomiasis, and schistosomiasis are neglected parasitic diseases for which new treatments are urgently needed. To identify new chemical leads, we screened the 400 compounds of the Open Access Malaria Box against the cysteine proteases, cruzain (*Trypanosoma cruzi*), rhodesain (*Trypanosoma brucei*) and SmCB1 (*Schistosoma mansoni*), which are therapeutic targets for these diseases. Whereas just three hits were observed for SmCB1, 70 compounds inhibited cruzain or rhodesain by at least 50% at 5 μM. Among those, 15 commercially available compounds were selected for confirmatory assays, given their potency, time-dependent inhibition profile and reported activity against parasites. Additional assays led to the confirmation of four novel classes of cruzain and rhodesain inhibitors, with potency in the low-to mid-micromolar range against enzymes and *T. cruzi*. Assays against mammalian cathepsins S and B revealed inhibitor selectivity for parasitic proteases. For the two competitive inhibitors identified (compounds **7** and **12**), their binding mode was predicted by docking, providing a basis for structure-based optimization efforts. Compound **12** also acted directly against the trypomastigote and the intracellular amastigote forms of *T. cruzi* at 3 μM. Therefore, through a combination of experimental and computational approaches, we report promising hits for optimization in the development of new trypanocidal drugs.

1. Introduction

The neglected parasitic diseases of poverty afflict millions of people in most developing countries and are a low priority in the pharmaceutical industry's research and development (R&D) programs. The available treatments present serious problems, such as low efficacy and high toxicity, leading in some instances to the discontinuation of treatment [1–3]. American Trypanosomiasis (Chagas disease) [1], Human African Trypanosomiasis (HAT, sleeping sickness) [2] and schistosomiasis (blood fluke) [3] are caused by *Trypanosoma cruzi*, *Trypanosoma brucei* and *Schistosoma mansoni*, respectively [4]. In the case of Chagas disease, there are no good treatments available for the chronic infection stage in which most patients are diagnosed. The world has recently watched

* Corresponding author. Laboratório de Modelagem Molecular e Planejamento de Fármacos, Departamento de Bioquímica e Imunologia, Instituto de Ciências Biológicas, Universidade Federal de Minas Gerais, Avenida Antônio Carlos 6627, Belo Horizonte, MG, 31270-901, Brazil.
E-mail address: rafaelasf@icb.ufmg.br (R.S. Ferreira).

https://doi.org/10.1016/j.ejmech.2019.06.062
0223-5234/

significant changes in the pattern of transmission and dissemination of these diseases, especially due to environmental and climate change events, and population mobility around the globe [5,6]. Thus, tropical diseases, once considered a common public health issue of developing countries, are gradually becoming a global health concern.

International efforts supported by public-private partnerships (PPPs) aim to achieve patients' needs by identifying and characterizing effective pharmaceutical tools to treat and cure tropical diseases. Important PPPs include the Medicines for Malaria Venture (MMV) [7], and the Drugs for Neglected Diseases initiative (DNDi). One of the strategies to accelerate drug discovery for neglected tropical diseases (NTDs) was the assembly of sets of freely available compounds, constituting chemical boxes distributed upon demand, such as the Malaria box [8], the GlaxoSmithKline kinetoplastid boxes [9], and the Pathogen box [7]. The Malaria Box is a set of 400 compounds (MMV400) displaying promising pharmacological activity against blood-stage *Plasmodium falciparum* under *in vitro* conditions [7,8]. Despite the initial focus on malaria, the library has already been explored as promising lead compounds against several pathogenic agents, including *T. cruzi*, *T. brucei* and *S. mansoni*, to identify new molecules capable of killing these parasites [10–14].

In the present study, we screened the MMV400 set against recombinant cruzain, rhodesain and SmCB1. These cathepsin L-like (cruzain and rhodesain) and cathepsin B-like (SmCB1) enzymes are essential cysteine proteases related to the development and survival of *T. cruzi*, *T. brucei* and *S. mansoni*, respectively. These proteins have been validated as pharmacological targets [15–20] and diverse inhibitor classes have been reported [19,21–38]. Here we identified two hits, MMV006169 (7) and MMV019918 (**12**), as competitive noncovalent inhibitors of cruzain and rhodesain. We show their chemical novelty when compared to known inhibitors, their selectivity towards trypanosomal proteases over mammalian cathepsins and activity against *T. cruzi*. Thus, they are new investigatory molecules for the treatment of trypanosomiasis.

2. Results

2.1. Primary screen and prioritization of hits for follow up

To identify potential inhibitors, the 400 compounds of the Open Access Malaria Box were initially screened at the concentration of 5 μM, in enzymatic assays against cruzain, rhodesain and SmCB1. Measurement of enzyme activity employed a fluorimetric assay in a 96-well plate format. Two assay conditions were considered; no pre-incubation and 10 min pre-incubation of the compounds with the enzymes. Seventy compounds inhibited at least one of the cathepsin L-like cysteine proteases (cruzain and rhodesain) by at least 50% at 5 μM (Fig. S1, Table S1). Among these, 39 were hits against both enzymes, 15 only against cruzain and 16 only against rhodesain, representing respectively 56%, 21% and 23% of all hits. Thus, the majority of hits for the cathepsin L-like enzymes overlapped, as expected based on their high sequence and structural similarity, including in their respective active sites, and on previously reported studies describing compounds that inhibit both enzymes [22,23,26,29,30,32–34,36,39,40]. It is worth noting that very few compounds were selective for either enzyme, as 23 out of the 31 molecules classified as hits for a single enzyme also displayed between 35 and 50% inhibition for the other trypanosomal enzyme.

In contrast to the high hit rate for the trypanosomal proteases, just three compounds were hits (over 50% inhibition at 5 μM) against the cathepsin B-like SmCB1 and another eight molecules inhibited this enzyme by at least 35% (Table S2). These did not overlap with the cruzain and rhodesain hits. Whereas the selectivity against cathepsin L-like versus cathepsin B-like enzymes might be expected due to sequence and structural differences, as SmCB1 has only 27–28% sequence identity to cruzain and rhodesain, the high difference in hit rates is a surprising result from this study. High standard errors were also observed for the few SmCB1 hits obtained, leading us, therefore, to focus on the inhibitors of cathepsin L-like proteases.

A comparison of inhibition profiles indicates a much higher hit rate under pre-incubation conditions, a likely indication of inhibition based on covalent ligand-protein interactions. Average percentages of inhibition were much higher under pre-incubation conditions (Fig. S1). To better evaluate time-dependence, we divided the hits into three categories, depending on whether the difference between percentages of inhibition with and without pre-incubation was: less than 25% (low time-dependence), between 25 and 50% (intermediate time-dependence), or more than 50% (high time-dependence). Most hits (51% of them) displayed intermediate time-dependence, while low and high time-dependent categories represented 24% of hits each.

Aiming to characterize potential inhibitors presenting a reversible and noncovalent mode of interaction with the cysteine proteases, which are less likely to affect off-targets, 15 compounds (Fig. 1) were selected from the first screen, primarily prioritizing molecules active against both trypanosomal proteases and which didn't display a high time dependence. Commercial availability, drug-likeness, synthetic feasibility to obtain derivatives and previously described *in vitro* or *in vivo* activities against *T. cruzi* and *T. brucei* [8] were also considered for compound selection (Table 1).

2.2. Biochemical characterization of prioritized hits

The 15 selected hits were purchased and evaluated for inhibition of cruzain and rhodesain (Table 2). Most compounds exhibited low activity in an initial evaluation at 10 μM, showing lower activity than in the initial screen (Table S3). Thus, to detect less potent inhibitors, compounds were also assayed at higher concentrations, ranging from 20 to 300 μM depending on their solubility at assay conditions. Based on these assays we selected seven compounds (compounds **2**, **5**, **6**, **7**, **8**, **12**, and **15**) for further study. The remaining eight hits (compounds **1**, **3**, **4**, **9-11**, **13** and **14**) showed only weak inhibition in the secondary screen and were not studied further.

Among the seven inhibitors chosen, we could measure activity for five cruzain inhibitors (IC_{50} values between 3 and 101 μM) and four rhodesain inhibitors (IC_{50} values between 9 and 52 μM) (Table 2). Analysis of the dose-response curves revealed a high Hill slope (3.9) for compound **6**, suggesting a super-stoichiometric mechanism [41]. Based on this evidence and on the high rate of aggregators among screening false positive hits [42,43], we investigated aggregation as a possible undesirable mechanism of enzyme inhibition, through two well-established assays [44–46]. First, hits were evaluated in two different Triton X-100 concentrations (0.01% and 0.1%) and in the absence of this detergent. Despite the fact that all previous assays had been performed in the presence of 0.01% Triton X-100, which is usually enough to prevent aggregate formation, it is known that some aggregates are more resistant to detergent [45,46]. Compounds **5**, **6** and **8** were highly sensitive to Triton, with reduced inhibition at higher detergent concentrations (Table S4) [44,46]. Also consistent with aggregation, inhibition by the same compounds was sensitive to pre-incubation with bovine serum albumin (BSA) (Table S4). Finally, compound **5** and **6** displayed fluorescence in the assays, which can be misinterpreted as inhibition by signal interference [30]. This fluorescence is expected due to the extended conjugation present in these compounds and its similarity to well-established fluorescent probes such as

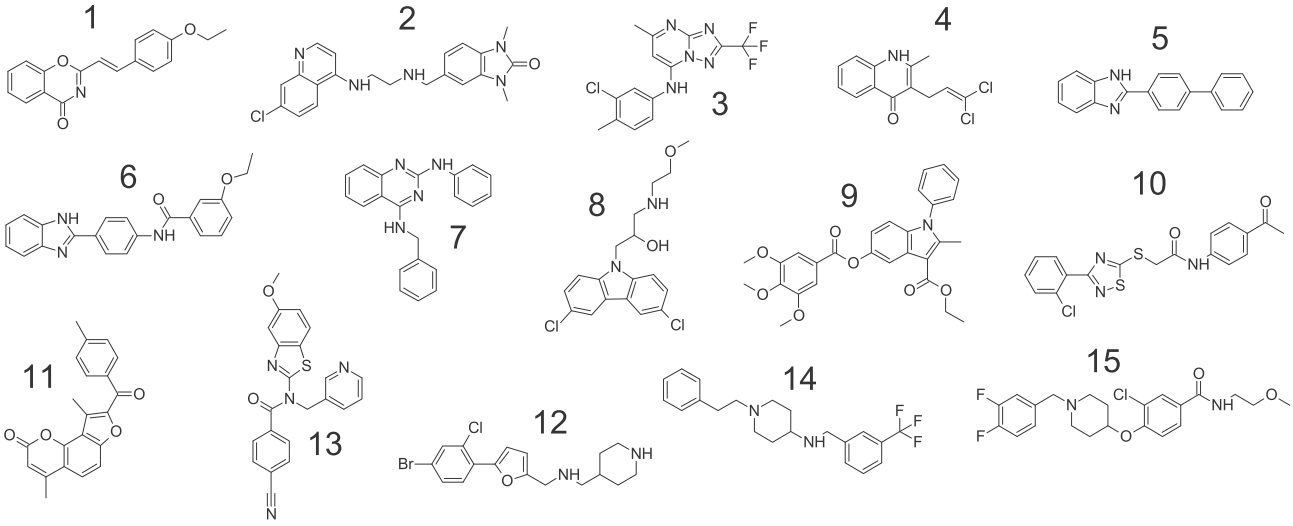

Fig. 1. Molecular structures of 15 potential inhibitors of cruzain and rhodesain selected after initial screening of the MMV400 set.

Table 1
Fifteen screening hits selected for characterization and their respective properties.

Compound	Time dependence[a]	Over 50% cruzain and rhodesain inhibition?	RO5 Classification[b]	Reported IC_{50}[c] against parasites (μM)		
				T. cruzi[d]	*T. brucei brucei*[e]	*T. brucei rhodesiense*[f]
1	high	yes	drug-like	17.8	32	30.5
2	intermediate	yes	drug-like	16.9	11.5	0.4
3	intermediate	no	probe-like	22.9	32	15.9
4	intermediate	yes	drug-like	1.9	32	32
5	low	yes	probe-like	32	32	32
6	low	yes	probe-like	32	32	32
7	low	yes	drug-like	1.5	3.4	3.1
8	intermediate	no	probe-like	3.9	0.7	0.4
9	intermediate	yes	drug-like	13.3	16.2	10.8
10	intermediate	yes	drug-like	32	32	32
11	low	yes	drug-like	32	32	32
12	intermediate	no	probe-like	1.0	0.1	0.1
13	intermediate	yes	drug-like	5.5	32	16.1
14	high	yes	probe-like	15.7	2.7	1.3
15	intermediate	yes	probe-like	32	32	16.1

[a] Hits were classified into three levels of time-dependence, depending on whether the difference between percentages of inhibition with and without pre-incubation was: less than 25% (low), between 25 and 50% (intermediate), or more than 50% (high).
[b] RO5, *Lipinski's* rule of five.
[c] Half Maximal Inhibitory Concentration.
[d] Data from PubChem Bioassay AID 660868, against *T. cruzi* Tulahuen C4 LacZ strain.
[e] Data from PubChem Bioassay AID 660869, against *T. brucei brucei* (Squib 427) strain.
[f] Data from PubChem Bioassay AID 660870, against *T. brucei rhodesiense* (STIB 900) strain.

Thioflavin T, commonly used to monitor protein aggregation [47]. Thus, **5**, **6** and **8** were not studied further.

Compound **15** was a relatively potent cruzain and rhodesain inhibitor, presenting IC_{50} values of 5 and 9 μM, respectively, when pre-incubated with the enzymes. However, a high time dependence was observed in assays against cruzain which potentially indicates covalent binding. Compound **2** inhibited both enzymes and displayed a low time dependence with better activity after pre-incubation with the enzymes (IC_{50} values around 51 and 38 μM against cruzain and rhodesain, respectively). Compounds **7** and **12** inhibited both enzymes in a non-time dependent manner with low to mid μM IC_{50} values against cruzain (9 and 26 μM, respectively) and rhodesain (30 and 53 μM, respectively).

Inhibition by compounds **2**, **7** and **12** were not time-dependent and in general not sensitive to detergent nor BSA incubation, although some detergent-sensitivity was observed for **7** at 50 μM (a concentration 5-fold higher than its IC_{50} against cruzain) (Tables 2 and S4).

We next determined the mechanism of inhibition of the trypanosomal enzymes by **2**, **7** and **12** at several substrate and inhibitor concentrations. Compound **2** revealed a mixed mechanism versus rhodesain ($K_i = 10$ μM), whereas for **7** and **12** a competitive inhibition against cruzain was observed ($K_i = 1.4$ and 3 μM, respectively), as determined based on Lineweaver–Burk plots (Fig. 2).

2.3. Chemical similarity analysis

To gain further insight into the novelty of compounds **2**, **7**, **12** and **15**, we sought to compare their chemical structures to known cruzain and rhodesain inhibitors. We constructed a library of 750 inhibitors from 64 cruzain studies and 516 structures from 46 rhodesain studies (Table S5).

The heatmaps generated from similarity matrices using Hashed fingerprints (Fig. 3) show a clustering pattern on most studies, both for cruzain and rhodesain inhibitors. Furthermore, a relatively low

Table 2
Secondary screening assays and characterization of selected compounds from MMV400.

Compound	CRUZAIN			RHODESAIN		
	Inhibition at highest screening concentration[a] (X ± SEM %)		IC_{50} (μM)	Inhibition at highest screening concentration[a] (X ± SEM %)		IC_{50} (μM)
	NI	I		NI	I	
1	15 ± 1	10 ± 1	nd	14 ± 2	0 ± 0	nd
2	75 ± 3	80 ± 2	145 ± 22 (NI) 51 (I)	67 ± 2	71 ± 1	38 ± 3 (I)
3	25 ± 2	16 ± 1	nd	16 ± 4	15 ± 6	nd
4	3 ± 2	7 ± 2	nd	4 ± 2	3 ± 1	nd
5	33 ± 2	38 ± 4	nd	14 ± 1	52 ± 5	nd
6	89 ± 2	100 ± 0	2.6 (NI)	46 ± 6	100 ± 0	nd
7	91 ± 1	90 ± 2	9 ± 2 (NI)	85 ± 6	94 ± 2	30 ± 4 (NI)
8	50 ± 2	67 ± 3	nd	38 ± 2	48 ± 1	nd
9	10 ± 5	19 ± 1	nd	4 ± 2	14 ± 4	nd
10	10 ± 2	23 ± 1	nd	10 ± 4	43 ± 4	nd
11	3 ± 2	11 ± 2	nd	8 ± 2	12 ± 2	nd
12	78 ± 1	84 ± 1	26 ± 1 (NI)	96 ± 1	75 ± 2	53 ± 2 (NI)
13	9 ± 1	7 ± 1	nd	10 ± 5	21 ± 4	nd
14	7 ± 2	22 ± 3	nd	12 ± 1	14 ± 4	nd
15	29 ± 3	78 ± 4	5 ± 1 (I)	63 ± 4	75 ± 2	9 ± 4 (I)

Notes: X, mean; SEM, standard error of the mean; nd, no determined; NI, no pre-incubation; I, 10 min of pre-incubation with the enzyme. Results were obtained from at least one assay in triplicate.
[a] Maximum solubility of compounds under test conditions: 2.5 μM (**11**), 10 μM (**5**, **6**, **9**, **10**, and **13**), 20 μM (**1** and **4**), 100 μM (**3**, **7**, **8**, **14** and **15**) and 300 μM (**2** and **12**).

off-cluster similarity can be seen with off-diagonal regions connecting studies exploring similar structures and moieties. This suggests a relatively well-explored chemical space, as various structural motifs are reflected in a mostly low similarity heatmap, as especially seen on the cruzain dataset. Similarity matrices of MACCS (Molecular ACCess System) fingerprints exhibit a similar pattern (Fig. S2). However, they produced higher Tanimoto coefficient values, as expected (Table S6 as a separate spreadsheet). The overall agreement between results for the two fingerprints, based on the different methodologies, indicates that they were able to capture the main data trends. Analysis of substances **2**, **7**, **12** and **15** suggests a low mean similarity to all known cruzain or rhodesain inhibitors. The highest Tanimoto coefficient value observed between any of these compounds and known inhibitors was 0.553, indicating significant structural differences even for this compound pair (Table S7).

To conduct an in-depth analysis beyond raw mean similarity, we used Hashed fingerprints data to construct similarity histograms for each of substances **2**, **7**, **12** and **15** to the dataset of all previously reported inhibitors (Fig. S3). In all histograms, the region representing similarity along all known inhibitors extends onto the higher similarity region, whereas in histograms for substances **2** and **7**, and especially for **12** and **15**, structures are seldom found in this region. Therefore, in this study, we describe a set of novel cruzain and rhodesain inhibitors, dissimilar to each other and known inhibitors, despite the previous description of several inhibitor classes for these enzymes.

2.4. Selectivity versus mammalian cathepsins

Next, we evaluated the selectivity of compounds **2**, **7** and **12**, when compared to the homologous cathepsins, human cathepsin S and rat cathepsin B. Cathepsin S is a cathepsin L-like enzyme as cruzain and rhodesain, with respectively 39 and 40% sequence identity. Also, cruzain and cathepsin B possess similar carboxydipeptidase activities and have in common a glutamate at the bottom of the S2 subsite, which allows for the recognition of positively charged groups in this pocket [48]. In addition, the catalytic domain of human and rat cathepsin B share 84% sequence identity and even greater identity of residues in the active site, and high structural similarity (overall Cα-RMSD 0.5 Å between human cathepsin B (Protein Data Bank (PDB) code 1GMY) and rat cathepsin B (PDB code 1THE)). At the highest concentrations tested (100 μM for **2** and **12**, and 50 μM for **7**), the greatest inhibition observed was 30% for cathepsin S by compound **12** and 29% for cathepsin B by compound **7**. In all other cases, the percentages of inhibition were under 15% (Table S8). These results suggest that compounds **2**, **7** and **12** are selective cruzain and rhodesain inhibitors, an important characteristic for lead compounds in the development of treatments for parasitic infections.

2.5. Binding mode prediction

The newly discovered inhibitors may be starting points for further optimization efforts. Accordingly, and given the availability of three-dimensional structural information for cruzain and rhodesain [29,33,49], we performed docking studies to understand the binding mode and ligand-protein interactions of competitive inhibitors **7** and **12** in the active site of both target enzymes. Protein flexibility was considered by employing the Glide Induced Fit Docking (IFD) Protocol [50]. To consider relevant protonation states during docking, theoretical pK_a calculations were performed for the ligands, indicating a pK_a of 6.86 for the N1 quinazoline ring in **7**. Therefore, two ionization states were considered for this compound. No other ionizable centers are predicted to have multiple relevant ionization states at pH 5.5 for **7** (Fig. S4). In turn, at pH 5.5, compound **12** was predicted to be protonated at both NHs encountered in its structure.

Similar binding modes were predicted for compound **7** interacting with both enzymes, regardless of its protonation state (Fig. 4A–D). The presence of two phenyl rings and a quinazoline ring on the structure of **7** suggested the prevalence of hydrophobic interactions to proteins. The accommodation of hydrophobic groups by the cruzain S2 subsite is well described in the literature [25,51], and the quinazoline ring is predicted to be enclosed by this pocket. For the protonated state of **7**, vicinal electrostatic interactions are also predicted between the S^- of Cys25, and the NH^+ and phenylamine NH, against both cruzain (distances of 2.6 and 2.0 Å, respectively, Fig. 4A) and rhodesain (distances of 2.9 and 2.2 Å, respectively, Fig. 4B). The benzylamine group is directed to the cruzain S3 pocket and the N4' of this group forms a hydrogen bond to the Leu160 main chain carbonyl (distance of 2.2 Å) while

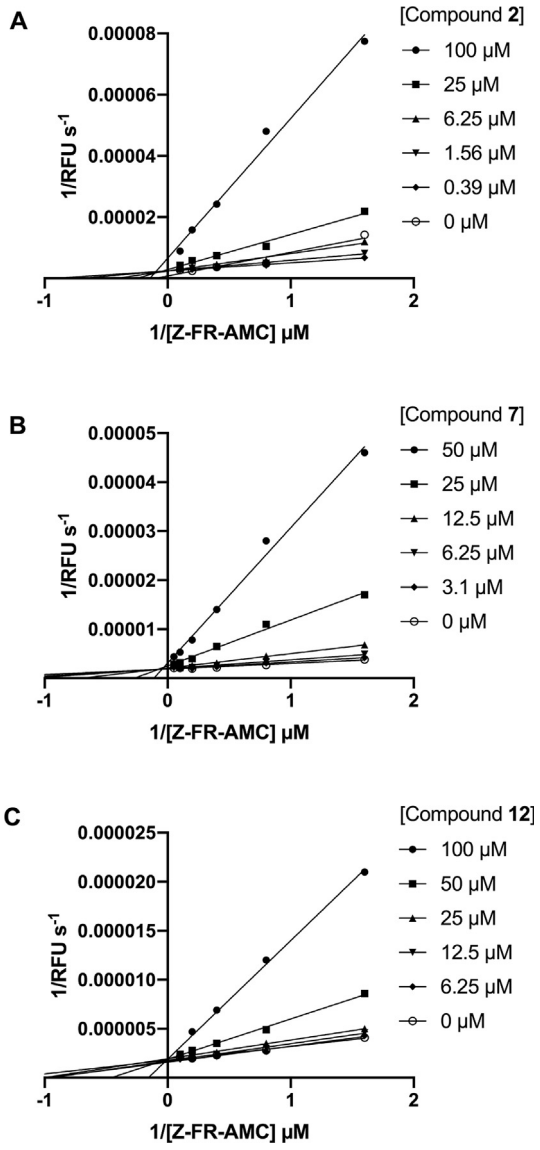

Fig. 2. Mechanism of enzyme inhibition by selected hits. Lineaweaver-Burk plots for compounds (A) **2** against rhodesain, (B) **7** against cruzain, and (C) **12** against cruzain. Compounds **7** and **12** displayed competitive behavior, as indicated by the same maximum velocity (V_{max}, y-intercept in graphs) in the presence of different inhibitor concentrations, while variation both in the maximum velocity and K^{app}_{m} (related to x-intercept in graphs) indicated that **2** is a mixed-type inhibitor. RFU, Relative Fluorescence Units.

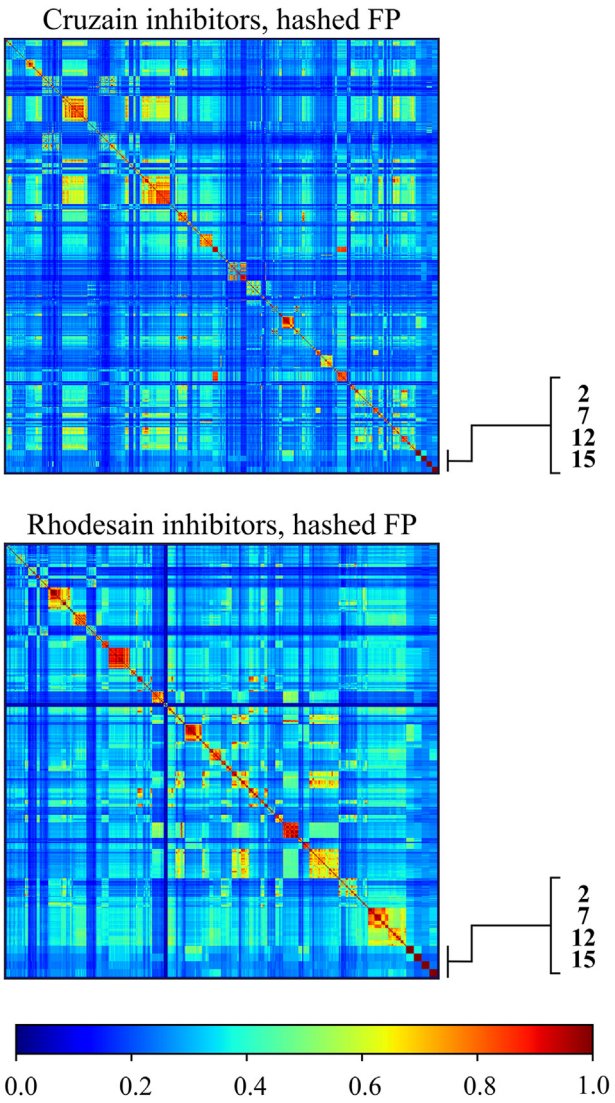

Fig. 3. Heatmaps generated from similarity matrices comparing known inhibitors of cruzain and rhodesain using hashed fingerprints. Novel inhibitors **2**, **7**, **12** and **15** are presented using a larger area for clarity.

the phenyl ring is mostly exposed to solvent. Against rhodesain, the benzylamine ring is slightly shifted and more solvent exposed, but still maintains a hydrogen bond to the Leu160 main chain carbonyl (distance of 2.1 Å) (Fig. 4B). The predicted pose for the deprotonated form of **7** against cruzain (Fig. 4C) differs significantly from that obtained for the protonated form solely for the absence of electrostatic interaction between quinazoline NH^{+} and Cys25. For rhodesain, the deprotonated form of **7** (Fig. 4D) is more deeply buried in the S2 pocket, which interacts with both quinazoline and phenylamine rings, while the benzylamine ring is exposed to the solvent and no hydrogen bonds nor electrostatic interactions were predicted.

The predicted binding modes for **12** against cruzain and rhodesain are very similar, and the main difference is the twisting on 2-chloro-4-bromo-phenyl ring, which shows the chlorine atom positioned inside the S2 cavity in case of cruzain (Fig. 4E) and exposed to solvent when docked against rhodesain (Fig. 4F). The chlorine atom interacts with the cruzain Leu67 main chain nitrogen through a dipole-dipole interaction (distance of 3.1 Å). Against both enzymes, the acyclic protonated amine (N1) and the hydrogen of piperidine's nitrogen (N8) interact with the backbone carbonyl and carbonyl side chain in Asp161 (distances of 1.7 Å and 1.7 Å for cruzain and 1.9 Å and 2.2 Å for rhodesain, respectively). Simultaneously, possible salt bridges were found between the acyclic protonated amine (N1) and Cys25 for cruzain and rhodesain (distances of 2.2 and 2.3 Å, respectively). As observed and discussed for compound **7**, a hydrophobic ring is enclosed in the S2 subsite.

2.6. Evaluation against Trypanosoma cruzi

Next, we investigated the trypanocidal activity of compounds **2**, **7**, **12** and **15**. Previous reports indicated their activity against *T. brucei* and the *T. cruzi* Tuhaluen 2 strain (Table 1). To further characterize activity against *T. cruzi*, we evaluated their activity against the Y strain, which is commonly employed for screening and is characterized by causing low parasitemia but high mortality

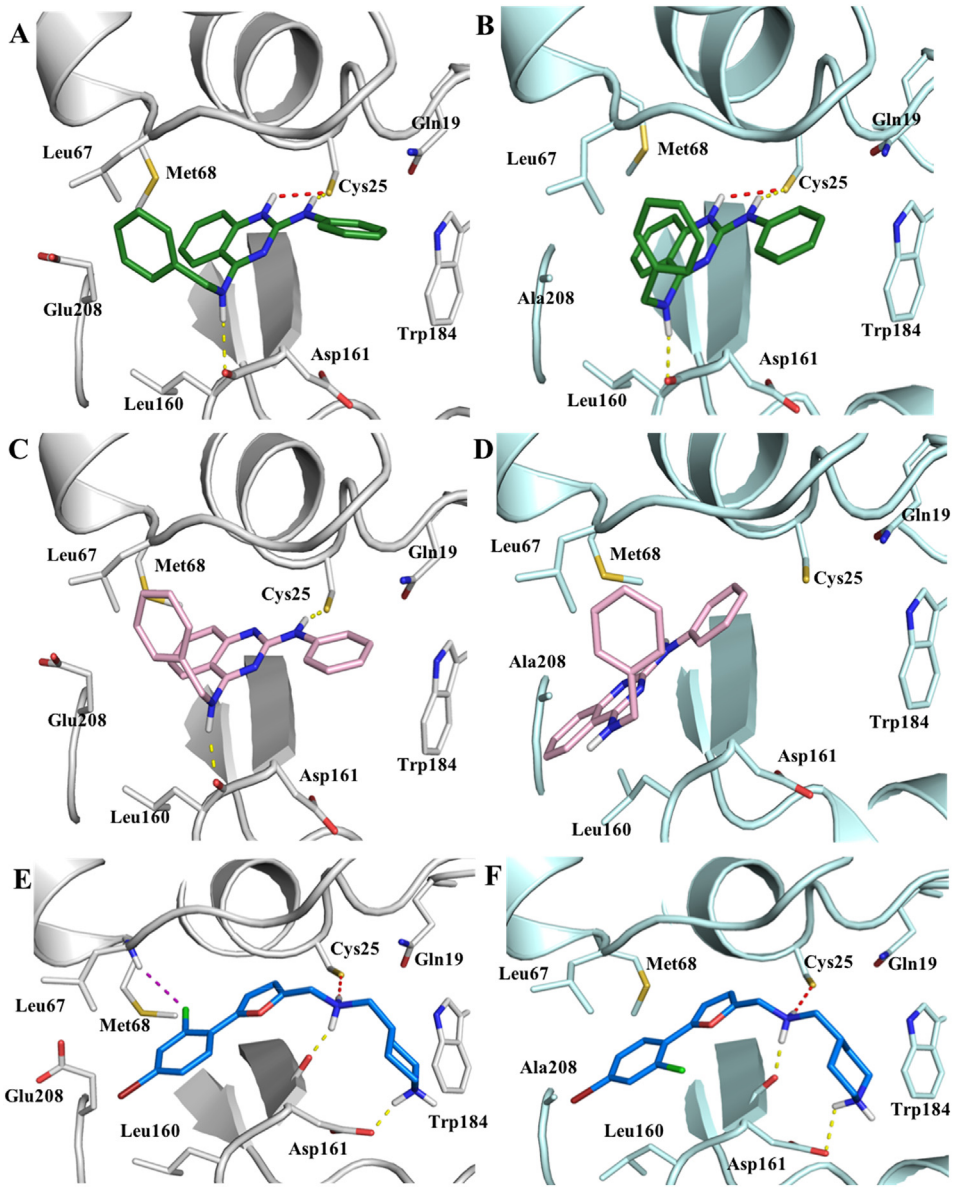

Fig. 4. Predicted binding modes for competitive inhibitors **7** and **12**. (A) Compound **7** protonated-cruzain. (B) Compound **7** protonated-rhodesain. (C) Compound **7** deprotonated-cruzain. (D) Compound **7** deprotonated-rhodesain. (E) Compound **12** -cruzain and (F) Compound **12** -rhodesain. Cruzain and rhodesain cartoon shown in gray and blue respectively. Hydrogen bond, dipole-dipole and electrostatic interaction are displayed as yellow, purple and red dashes, respectively. Selected residues of the active site are highlighted as sticks. The figure was prepared using PyMOL. (For interpretation of the references to colour in this figure legend, the reader is referred to the Web version of this article.)

in mice depending on their background [52]. An initial screen with these compounds at 50 μM revealed trypanocidal activity for all of them (Fig. S5). These assays indicated that compound **12** had good trypanocidal activity, inhibiting trypomastigote release at 3.125 μM, and low toxicity against murine macrophages, and it was, therefore, chosen for more detailed studies.

We then studied the effect of compound **12** on *T. cruzi* in infected macrophages. Macrophages are innate immune cells that play an important role in controlling the replication of parasites and stimulating adaptive immunity cells. In peritoneal macrophages exposed to *T. cruzi* infection and treated with **12** in a dose-response manner, we measured a decrease in the release of trypomastigote forms relative to their controls at all concentrations tested, and with activity similar to those treated with IFN-γ (Fig. 5A). In the cell viability test, based on measurement of lactate dehydrogenase (LDH), 3.125 μM of **12** did not exhibit cytotoxic activity as the LDH levels were equivalent to those detected in the supernatant of the macrophages incubated with IFN-γ or medium alone (Fig. 5B).

To investigate the possible direct action of **12** on the extracellular trypomastigote forms, the parasites were incubated with 3.125 μM **12**. There was a significant reduction (77% reduction) in the number of trypomastigote forms after 1 h when compared to vehicle controls, indicating the direct action of the compound on the parasites (Fig. 5C). Next, the trypomastigotes that survived after 1 h of incubation with **12** or medium alone were used to infect the macrophages. The intracellular replication of **12**-treated parasites was reduced when compared with untreated parasites (Fig. 5D). For example, the number of trypomastigotes released 7 days after infection was 60% smaller for **12**-treated parasites. The LDH viability test demonstrated reduced macrophage damage upon

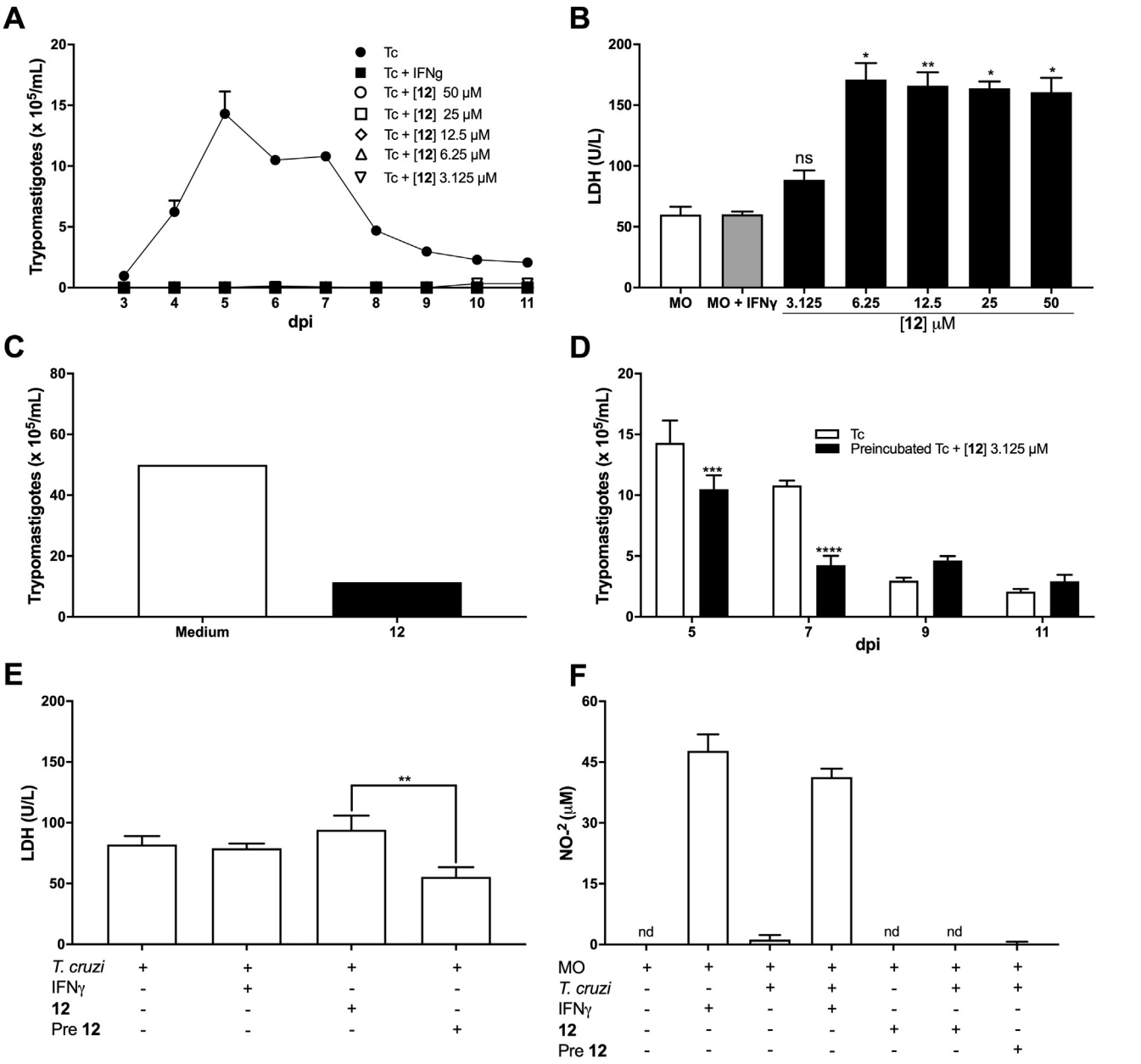

Fig. 5. Compound **12** acts both in the *T. cruzi* and host cells reducing the parasite load *in vitro*. Peritoneal macrophages of C57BL/6 mice were cultured and infected with *T. cruzi* trypomastigote forms at the ratio of 5:1 (parasite/cell) and stimulated or not, with IFNɣ ([IFNɣ] = 100 ng/ml) or **12** ([**12**] = 3.125, 6.25, 12.5, 25 and 50 µM). Parasite growth was measured by counting trypomastigote forms released in the supernatant at different times after infection (A). Cell damage was evaluated by measuring Lactate dehydrogenase (LDH) levels in the medium after 24 h of treatments with the different concentrations of **12** (B). (C) Number of trypomastigote forms before and after incubation with [**12**] = 3.125 µM for 1 h. (D) Counting trypomastigote forms released in the supernatant of macrophages after infection with trypomastigotes preincubated or not with ([**12**] = 3.125 µM) at 5, 7, 9 and 11 days after infection. (E) Cell damage measured by LDH cytotoxicity assay in the medium of macrophage after 24 h of infection with trypomastigote forms preincubated or not with [**12**] = 3.125 µM or macrophage treated with 12 after *T. cruzi* infection in the same concentration. (F) Nitric Oxide measured by Griess method in the culture supernatant after 11 days. (Data expressed as a mean+/-SEM, from three independent experiments, each performed in triplicates – Two-way ANOVA, post test Sidak; One-way ANOVA, post test Dunnett: ****p‹0.0001, ***p < 0.001, **p < 0.01, *p < 0.05; nd = not detected).

infection with parasites previously treated with **12** as compared to macrophages treated or not with **12**, or IFN-γ, and infected with untreated parasites (Fig. 5E). Compared to these conditions, pre-treatment with **12** reduced by approximately 30% LDH release. Altogether, these results suggested that **12** acts both on the host and parasite cells controlling the replication and release of *T. cruzi in vitro*. The increased trypanocidal activity induced by **12** was not related to an increase in nitric oxide production because the levels of NO was only increased in the presence of IFN-γ (Fig. 5F). Thus, the trypanocidal activity of **12** is independent of NO release.

2.7. Chemistry

To perform assays against *T. cruzi*, an additional quantity of **12** was required, and preparation was accomplished straight-forward following procedures described in the literature [53,54]. The first step consisted of a Meerwein reaction between 2-furancarboxaldehyde and the corresponding diazonium salt of 4-bromo-2-chloroaniline, prepared *in situ* with of $NaNO_2$ in aqueous HCl solution while keeping the reaction temperature below 0 °C. The coupling of the substituted furfural **16** with 4-

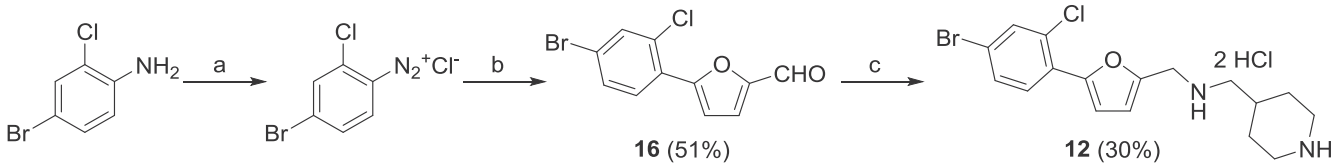

Scheme 1. Synthesis of compound **12**[a]
[a]Reagents and conditions: (a) (i) HCl 15% v/v, 0 °C, 10 min (ii) $NaNO_2$ (1.4 equiv), 0 °C, H_2O, 30 min, (b) 2-furancarboxaldehyde (1.2 equiv), $CuCl_2.2H_2O$ (0.15 equiv), rt, H_2O, overnight; (c) (i) 4-(aminomethyl)piperidine (1.2 equiv), Na_2SO_4 (6 equiv), CH_2Cl_2, rt, overnight, (ii) $NaBH_4$ (2 equiv), THF/metanol, rt, 4 h, (iii) ethereal HCl.

(aminomethyl)piperidine was achieved by reductive amination, using $NaBH_4$ as reducing agent, added after formation of the corresponding imine overnight. The amine obtained was purified by column chromatography and treated with an ethereal hydrochloric acid solution to obtain **12** as its more stable dihydrochloride salt (Scheme 1). All starting reagents were available commercially.

3. Discussion

Here we describe the screen of a privileged set of compounds towards the discovery of new leads for Chagas disease, HAT and schistosomiasis. A high hit rate was observed in the biochemical screen against cruzain and rhodesain, but not SmCB1. Approximately 12% of all compounds were able to inhibit at least 50% activity of cruzain and rhodesain in the primary screen [43]. Similarly, a high hit rate was also reported for a quantitative high-throughput screening (qHTS) campaign against cruzain, in which 8% of the 198 k compound library displayed cruzain inhibition in the initial screen. The higher hit rate in our study may be due to the evaluation also in pre-incubation conditions, as most hits were shown to be time-dependent. Also, only one compound concentration was evaluated in this study, while the qHTS allows better initial compound filtering based on dose-response curves.

Taking into account the high false-positive rates commonly reported in experimental screens and practical limitations regarding the number of compounds we could follow up with, an important step was the selection of 15 compounds for further characterization, when several properties relevant for drug development were considered. Among the selected molecules, 8 out of 15 could not be confirmed in secondary assays. This indicates a high false-positive hit rate from the primary screen, but it is consistent with reports from previous studies. In a study from Peev and collaborators, involving screening against three kinetoplastids to assemble the GlaxoSmithKline (GSK) kinetoplastid boxes, only around 50% of hits could be confirmed on each case, even though the same assays were employed in primary and secondary screenings [9]. Later, Salas-Sarduy and collaborators screened the GSK chemical boxes against cruzain and reported confirmation of only six out of fifteen hits in follow up assays [55].

Among the seven inhibitors further validated, three displayed aggregation behavior. The final four compounds were characterized as mixed type (**2**), competitive (**7** and **12**) or time-dependent (**15**) cysteine protease inhibitors. Our results are important for Chagas disease and HAT, especially given that the MMV400 compounds constitute a set of pre-filtered molecules with publicly available information. Additional advantages of employing the MMV400 are their free availability and the associated large dataset from a diversity of assays. Positive results from screening selected compounds sets have been reported in several cases, and highlight their potential for drug repurposing. For example, many new activities, unrelated to malaria, have been discovered by screening the MMV400 [14], and screening of the GSK HAT chemical box revealed compounds active against cruzain [55].

Among the several reports of activity for the MMV400, a number are particularly related to our study. Kaiser et al. performed screening against *T. cruzi*, *T. b. rhodesiense*, *T. b. brucei* and *L. infantum*, and trypanocidal compounds were identified. Among these, analogs of **7** and **12** were selective and active against *T. b. rhodesiense*, demonstrating the potential of the 2,4-disubstituted quinazoline and phenylfuran classes [11]. Another *in vitro* screen of the MMV400 led to new chemotypes that inhibited rhodesain and *T. brucei* at sub-micromolar concentration, and with low toxicity against Hep G2 cells at 20 μM [12]. It is interesting to note the difference in hits obtained in that study and the ones reported herein. To select our fifteen hits from the primary screen, we considered the inhibitory activity against two trypanosomal enzymes (cruzain and rhodesain) and compounds that did not display high time dependence, whereas in the above study the compounds were prioritized considering only their activity against rhodesain after pre-incubation with the enzyme. Therefore, despite screening the same compound set against the same target, differences in the study workflows make our study complementary to the previously reported, and led to the discovery of additional hits. Another interesting aspect observed in that study is the presence of benzimidazole ring in the molecules evaluated, a motif also present in compound **2**, a mixed-type inhibitor against rhodesain ($K_i = 10$ μM) and present in a series of rhodesain inhibitors that were recently characterized by our group [56,57].

Our docking studies provide a hypothesis concerning the selectivity of compounds **7** and **12** towards trypanosomal cathepsin L-like enzymes, in which the interaction in the S2 subsite appears to be the predominant specificity-defining factor. Previous studies demonstrated that the SmCB1 S2 pocket accommodates bulky hydrophobic residues such as Phe and Leu well, however, replacement by larger groups or with bulky substituents such as Phe-4-CH_3 or Phe-3-CF_3 reduces both potency against the enzyme and severity of impact against the parasite [31]. The selectivity of **7** and **12** might be due to differences in the S2 pocket, which is considerably smaller in SmCB1, in a way that hinders favorable binding modes against SmCB1 [31,58]. Similarly, cathepsin S prefers aliphatic amino acids and branched hydrophobic residues at the P2 position compared to aromatic residues due to the presence Phe205 in the S2 pocket which determines this specificity [58,59].

In addition to their activity against cysteine proteases, it is key to demonstrate compound activity against parasites. As described above, the MMV400 had already been screened against *T. brucei* and *T. cruzi* Tuhaluen 2 strain. However, it is well known that *T. cruzi* strains are highly heterogeneous concerning several properties, including drug susceptibility [52], enzyme activity levels [60,61] and infectivity rates [60]. Therefore, we sought to characterize compound **12**, which was the most potently trypanocidal against *T. cruzi* Y strain. In addition to demonstrating activity against this strain, our studies show that the trypanocidal activity of **12** is due to an effect(s) on multiple stages of the parasite replication cycle, including direct action on trypomastigote forms, reduction of intracellular parasite (amastigote form) replication and release by macrophages. Importantly, the LDH viability test demonstrated that compound **12** is not cytotoxic for macrophages.

To conclude, compounds **7** and **12** are novel competitive inhibitors of cruzain and rhodesain, and represent promising starting points for the development of small molecule treatments for Chagas disease and HAT. We are currently working on the structure-based optimization of these two compound classes.

4. Conclusions

Evaluation of the MMV400 against the major cathepsin L-like proteases of *T. cruzi* and *T. brucei* as well as the cathepsin B-like enzyme of *S. mansoni* led to the discovery of novel enzyme inhibitors. Compound **2** was identified as a novel mixed rhodesain inhibitor ($K_i = 1.4\,\mu M$). Compounds **7** and **12** showed low-micromolar potency against cruzain ($K_i = 1.4$ and $3\,\mu M$, respectively) and modest activity against rhodesain ($IC_{50} = 30$ and $50\,\mu M$, respectively). They also are new noncovalent competitive and selective inhibitors for trypanosomal cathepsin L-like proteases and are active *in vitro* against the *T. cruzi* Y strain. Therefore, they represent starting points for the structure-based optimization and development of cruzain and rhodesain inhibitors as new drug candidates for the treatment of trypanosomiasis.

5. Experimental section

5.1. Compounds

The 400 compounds from the Open Access Malaria Box [41] were supplied in 96-well plates containing frozen solutions (20 μL, 10 mM) in dimethylsulfoxide (DMSO). Solid samples for the following compounds were purchased from Ambinter: MMV665940 (**1**, Amb19544542), MMV665875 (**2**, Amb19787487), MMV665874 (**3**, Amb69119), MMV665994 (**4**, Amb1771002), MMV665891 (**5**, Amb6343408), MMV019202 (**6**, Amb6566900), MMV006169 (**7**, Amb673569), MMV019017 (**8**, Amb1291555), MMV396664 (**9**, Amb1264811), MMV666124 (**10**, Amb4182850), MMV086103 (**11**, Amb19794162), MMV019918 (**12**, Amb1095348), MMV001239 (**13**, Amb5231017), MMV665979 (**14**, Amb10816165) and MMV666072 (**15**, Amb11065479). Ambinter purchased compounds are assured to have >90% purity and were evaluated by NMR, mass spectrometry, IR spectrometry, UV–Vis spectrometry and elemental analysis.

5.1.1. Synthesis and characterization of compound 12

All reagents of analytical grade were obtained from commercial suppliers and used without further purification. The melting points were determined on a Microquímica MQAPF 301 apparatus. The FT-IR spectra were recorded using a PerkinElmer Spectrum One infrared spectrometer and absorptions are reported as wave numbers (cm^{-1}). The NMR spectra were recorded on a Bruker AVANCE DRX400 instrument, using tetramethylsilane (TMS) as the internal standard or solvent peak(s) of $CDCl_3$ (7.27 and 77.23 ppm) or CD_3OD (3.31 and 49.0 ppm). Data for ^1H NMR spectra are reported as follows: chemical shift (δ ppm), multiplicity, coupling constant (Hz), and integration. Splitting patterns are designated as follows: s, singlet; d, doublet; dd, doublet of doublets; m, multiplet; br, broad. The purity of the final compound was determined to be ≥ 95% by UHPLC (Shimadzu Nexera; column: Shimadzu Shimpack XR-ODSIII, C18, 2.2 μm, 80 Å, 2.0 × 150 mm). High-resolution mass spectra (HRMS) was acquired in positive mode using ESI as the ionization type (Bruker maXis ETD).

*5.1.1.1. 5-(4-Bromo-2-chlorophenyl)-2-furancarboxaldehyde (**16**) [54].* Initially, the diazonium salt of 4-bromo-2-chloroaniline was prepared as described in the literature, using HCl 15% and dropwise addition of an aqueous solution of $NaNO_2$ (1.4 equiv) while maintaining the reaction temperature below 0 °C. Subsequently, 2-furancarboxaldehyde (1.2 equiv) and $CuCl_2.2H_2O$ (0.15 equiv) were added to the solution and the reaction kept at room temperature overnight. The reaction was extracted with CH_2Cl_2 and washed with distilled water, a saturated $NaHCO_3$ solution and distilled water once again. The organic layer was dried over Na_2SO_4, filtered, and concentrated under reduced pressure. After workup, the crude was recrystallized with isopropanol to afford compound **16** as a pale-yellow solid (698 mg, 51% yield). mp: 153.5–154.6 °C. IR (neat, cm^{-1}): 3158, 3100, 2839, 1677, 1663, 1580, 1510, 1456. ^1H NMR (400 MHz, $CDCl_3$): δ 9.70 (s, 1H), 7.89 (d, $J = 8.4$ Hz, 1H), 7.66 (d, $J = 2.0$ Hz, 1H), 7.51 (dd, $J = 8.4$, 2.0 Hz, 1H), 7.35 (d, $J = 3.6$ Hz, 1H), 7.32 (d, $J = 3.6$ Hz, 1H). ^{13}C NMR (101 MHz, $CDCl_3$) δ 177.6, 154.6, 151.8, 133.7, 132.4, 130.8, 130.2, 126.8, 123.767, 123.1, 113.7.

*5.1.1.2. 1-[5-(4-Bromo-2-chlorophenyl)-2-furyl]-N-(4-piperidinylmethyl)methanamine dihydrochloride (**12**) [53].* To a solution of **16** in CH_2Cl_2 were added 4-(aminomethyl)piperidine (1.2 equiv) and Na_2SO_4 (6 equiv.). The reaction was kept at room temperature overnight and then filtered, the solvent removed under reduced pressure and replaced by a 3:1 mixture of THF/methanol, followed by addition of $NaBH_4$ (2 equiv.) in an ice bath. The reaction was magnetically stirred at room temperature for 4 h while being monitored by TLC and then quenched with a 1 M NaOH solution. After extraction with CH_2Cl_2, the organic layer was dried over Na_2SO_4, filtered, and concentrated under reduced pressure followed by separation by column chromatography with neutral alumina (eluent: CH_2Cl_2/methanol 0.5% + NH_4OH 0.5%). After purification, the product was solubilized in diethyl ether and precipitated as its dihydrochloride salt by adding an ethereal HCl solution. After solvent evaporation **12** was obtained as a pale-yellow solid in an average 30% yield. mp: 208–210 °C. IR (neat, cm^{-1}): 3378, 2951, 1611, 1582, 1465, 1207, 1087. ^1H NMR (400 MHz, MeOH-d_4): δ 7.89 (d, $J = 8.4$ Hz, 1H), 7.71 (d, $J = 1.2$ Hz, 1H), 7.59 (d, $J = 8.4$ Hz, 1H), 7.19 (d, $J = 3.2$ Hz, 1H), 6.86 (d, $J = 3.2$ Hz, 1H), 4.43 (s, 2H), 3.44 (d, $J = 12.8$ Hz, 2H), 3.11–3.00 (m, 4H), 2.19 (br s, 1H), 2.07 (d, $J = 14.0$ Hz, 2H), 1.65–1.51 (m, 2H). ^{13}C NMR (101 MHz, MeOH-d_4) δ 152.3, 146.3, 134.2, 132.2, 131.7, 130.7, 128.8, 122.8, 116.1, 113.6, 52.7, 44.8, 44.4 (2C), 32.4, 27.5 (2C). HRMS (ESI): (m/z) 383.0521 $[M+H]^+$, calcd 383.0520$C_{17}H_{20}N_2OBrCl$ (free base). The ^1H NMR for this compound, together with the assignment of each peak is shown as Fig. S6.

5.2. Expression and purification of cysteine proteases

Recombinant cruzain was kindly provided by Allison Doak and Dr. Brian K. Shoichet, from the University of California San Francisco, California, USA. Recombinant rhodesain and SmCB1 were expressed and purified as previously described [31,62,63]. Recombinant human cathepsin S was expressed, purified and activated as previously described [64], while rat cathepsin B was gently provided by Dr. Lukas Mach (BOKU Vienna).

5.3. Assays against cruzain, rhodesain and SmCB1

In vitro activity of trypanosomal cysteine proteases was assayed as previously described [30]. Enzymatic activity was measured by monitoring the cleavage of a fluorogenic substrate, Z-Phe-Arg-amidomethylcoumarin (Z-FR-AMC). Fluoresce was monitored at 340/440 nm excitation/emission for 5 min at 12s intervals for cruzain and rhodesain kinetics, and for 30 min at 23s intervals for SmCB1 kinetics, in a Synergy2 Biotek plate reader using BioTek's Gen5™ Reader Control and Data Analysis Software. Assays against cruzain and rhodesain were carried out using 2.5 μM substrate ($K_m = 0.5 \pm 0.1\,\mu M$ against cruzain and $K_m = 0.5 \pm 0.1\,\mu M$ against

rhodesain) and 1 nM enzyme in sodium acetate buffer 0.1 M, pH 5.5, containing 0.01% Triton X-100 and 1 mM β-mercaptoethanol. In parallel, assays against SmCB1 were performed using 20 μM substrate ($K_m = 12 \pm 1$ μM) and 8 nM enzyme in sodium acetate buffer 0.1 M, pH 5.5, containing 0.01% Triton X-100 and 4 mM β-mercaptoethanol. Negative and positive controls (DMSO and E-64, respectively) were employed in all assays. Reported values correspond to the mean and standard error of the mean of experiments performed in triplicate. This assay was performed for compound screening, IC_{50} determination, mechanism of inhibition and aggregation assays, with slight differences as described below.

5.4. Compound screening, IC_{50} values determination and mechanism of inhibition

The MMV400 was initially screened at 5 μM against the three recombinant proteases. Experiments were performed at two conditions: (i) no enzyme-compound pre-incubation and (ii) 10 min enzyme-compound pre-incubation, in two duplicates at each condition. Afterward, fifteen compounds were selected for a secondary screening, considering the percentage of inhibition in the first screening greater than 50% inhibition against both trypanosomal cathepsins and meeting criteria such as commercial availability, synthetic feasibility and previously described bioactivity.

Confirmatory (secondary) screening with the fifteen compounds selected was carried out at higher concentrations, which differed according to solubility limitations under assay conditions: 2.5 μM (**11**), 10 μM (**5**, **6**, **9**, **10**, and **13**), 20 μM (**1** and **4**) 100 μM (**3**, **7**, **8**, **14** and **15**) and 300 μM (**2** and **12**). IC_{50} values were obtained for compounds presenting inhibition higher than 70% in the secondary screening. At least two independent IC_{50} assays were performed, each using at least six compound concentrations in triplicate. IC_{50} curves were determined by nonlinear regression analysis using GraphPad Prism 6 [65].

To determine the mechanism of inhibition and K_i values, cruzain and rhodesain activities were monitored at least six different substrate concentrations (0.3–20.0 μM) and five inhibitor concentrations (variable depending on compound potency). Results were calculated by nonlinear regression of (i) log(inhibitor) vs response - *variable slope* (four parameters), (ii) Enzyme Kinetic - Substrate vs Velocity (*Michaelis Menten*) and (iii) linear regression (*Lineweaver-Burk plots*) using GraphPad Prism 6 [65].

5.5. Aggregation assays

Assays were performed as described above, with the following modifications. To evaluate detergent sensitivity, cruzain was pre-incubated with compounds for 10 min at room temperature in the absence and in the presence of Triton X-100 (0.1% and 0.01%) [45,46]. Percentages of enzyme inhibition at these different Triton concentrations were compared.

In an additional assay, compounds were incubated for 5 min with BSA (2 mg/mL in Triton X-100 0.001%) followed by 5 min incubation in the presence of 1 nM cruzain, and then addition of substrate solution and monitoring of enzyme activity [44,45]. For comparison, assays were performed in parallel in the absence of BSA and otherwise identical conditions.

5.6. Evaluation against mammalian cathepsins (human cathepsin S and rat cathepsin B)

Proteolytic activity was determined as previously described, using substrates CBZ-Val-Val-Arg-7-amido-4-methylcoumarin (Z-VVR-AMC) for cathepsin S and CBZ-Phe-Arg-amidomethylcoumarin (Z-FR-AMC) for cathepsin B, with the release of fluorescent 4-amino-7-metyhlcoumarin monitored in an Infinite 200 PRO microplate reader of the Structural Biology Group of Universität Salzburg. Fluorescence was monitored employing 380 nm wavelength for excitation and 460 nm or 440 nm wavelength for emission (460 nm in the cathepsin S assays and 440 nm in the cathepsin B assays). All assays were performed in 96-well black plates, without and with pre-incubation (5 min) of the compounds with the enzyme. Compounds **2** and **12** were assayed at 100 μM while **7** was assayed at 50 μM. For each compound, two independent experiments were performed, each in triplicate and monitored for 15 min. Percentage of inhibition was calculated by comparison to a DMSO control (final concentration of 2%). Cysteine protease inhibitor E64 (1 μM) was used as a positive control of inhibition. Cathepsin S assays were performed at 37 °C, in a final volume of 55 μL of 50 mM sodium acetate buffer, 100 mM sodium chloride, 5 mM ethylenediaminetetraacetic acid (EDTA), 2 mM Dithiothreitol (DTT), pH 5.5, in the presence of 5 nM enzyme and 50 μM of Z-VVR-AMC ($K_m = 107 \pm 11.3$ μM, similar to the value reported in a previous study ($K_m = 102.2 \pm 1.52$ μM) [66]. Cathepsin B assays were performed at 25 °C in a final volume of 50 μL of 100 mM sodium phosphate buffer, 100 mM sodium chloride, 1 mM EDTA, 1 mM DTT and 0.01% CHAPS, (3-((3-cholamidopropyl) dimethylammonio)-1-propanesulfonate), in the presence of 20 nM enzyme and 50 μM of Z-FR-AMC ($K_m = 22.3 \pm 8$ μM) [67].

5.7. Docking studies

Preparation of ligands (**7** and **12**), proteins (cruzain and rhodesain) and docking calculations were performed using the Maestro unified interface, by the Schrödinger Small Molecule Discovery Suite [68]. LigPrep was used to obtain ionization states for **7** and **12**, by Epik program at pH 5.5, optimizing conformations by MMFF force field [69–72]. The PDB structures employed for docking were cruzain PDB ID 3KKU [29] and rhodesain PDB ID 2P86 [73]. All structures employed consist of complexes with inhibitors. These proteins were prepared by using the Protein Preparation tool [74,75], considering calculations of residues' protonation states at pH 5.5 using PROPKA. In addition to PROPKA calculations, two changes were performed on the structure of proteins: deprotonation of Cys25 and protonation of His162, forming an ion-pair at the catalytic site responsible for the hydrolytic activity [76,77], and the Glu208 residue on S2 pocket cruzain was also deprotonated. All waters and ligands were removed from all protein structures. Grids were generated on Glide and defined as all atoms within a distance of 12 Å from the catalytic cysteine sulfur atoms (*Glide, version 6.8*) [78–80]. Docking studies inducing conformational changes in active sites of proteins were performed with the Induced Fit Docking protocol [50,81]. Initial docking was performed using Glide SP, ligand van der Waals radii of both receptor and ligand were scaled to 0.5. The maximum of 20 poses per ligand were generated. Protein conformations were then generated with Prime, considering flexible all residues within 5 Å from ligand poses, and the conformations whose energy was up to 30 kcal/mol from the best structure and classified within the first 20 poses were selected for redocking. The final IFD redocking round was then performed with Glide XP [50,81]. Figures were prepared with Pymol [82].

5.8. Chemical similarity analysis

Structures of previously described cruzain and rhodesain competitive inhibitors were obtained PubChem, ScienceDirect, and from the BindingDB database [83] and compounds with IC_{50} or K_i up to 100 μM were considered. To search for studies reporting cruzain or rhodesain inhibitors, all papers containing either "cruzain" or "rhodesain" on either PubChem or ScienceDirect were

verified. To manually curate this data, compounds which were reported as detergent-sensitive inhibitors, aggregators and or unspecific inhibitors were discarded. Chemical structures from BindingDB were manually verified against references. Structures of MMV400 compounds were obtained from its supporting information. Fingerprints were calculated using either 166-bits MACCS fragments [84] or a Hashing algorithm, both through the implementation in RDKit.[85] Hashing fingerprint was generated using a topological linear algorithm and Daylight-like atom types with two up to seven atoms fragments. Tanimoto coefficient of each pair was calculated and similarity matrices were generated through a Python implementation. Similarity matrices were also used to generate heatmaps and histograms. Heatmaps were generated directly from unnormalized data, while diagonal elements were discarded to prepare histograms and calculate means.

5.9. T. cruzi culture

T. cruzi (Y strain) trypomastigote forms were cultured on *Macaca mulatta* fibroblast cells line (LLCMK2) in culture flasks (TPP®) with *Roswell Park Memorial Institute* 1640 medium (RPMI) supplemented with 5% fetal bovine serum, 1% L-glutamine (200 mM) and 1% penicillin and 1% streptomycin (RPMIc).

5.10. Animals

Wild-type (WT) C57BL/6 female mice, between 8 and 10 weeks old, were obtained from the Animal Care Facilities of UFMG, Minas Gerais, Brazil.

5.11. Macrophage culture

Macrophages (MO) were isolated from the peritoneal cavity of female C57BL/6 mice 72 h after the injection of 2 mL of sterile sodium thioglycolate 3%. Cells were collected by the wash of peritoneal cavity using sterile, frozen phosphate-buffered saline (PBS), centrifuged at 290×*g* for 10 min, resuspended in a volume of 1 ml of medium (RPMIc). Cells were counted in Neubauer's chamber for plaque of 2×10^5 macrophages/mL/well in a 96-well plate and incubated at 37 °C, 5% CO_2 for 3 h for adherence. After this period the wells were washed and left overnight for further stimuli. Three independent experiments were performed, with three mice employed in each.

5.12. Infection of the macrophages

Culture medium containing the parasites were withdrawn from the culture flask and centrifuged for 5 min at 50×*g* and the supernatant collected, then centrifuged at 2438×*g* for 10 min, the supernatant was discarded and the pellet resuspended in 1 mL of RPMIc. The parasites were counted in Neubauer's chamber for infection of the macrophages plated in the 96-well plate. Macrophages were infected in a ratio of 5:1 (parasite:cell) for 2 h at 37 °C, 5% CO_2, then the extracellular parasites were washed with RPMIc.

5.13. Macrophage stimulation with compound 12

Non-infected or *T. cruzi*-infected macrophages were stimulated with **12**at concentrations of 3.125, 6.25, 12.5, 25 and 50 μM (dose-response curve) or with IFN-γ (100 ng/mL - Sigma) and maintained throughout the remainder of the oven experiment at 37 °C, 5% CO_2. After 24 h 20 μL of supernatant was withdrawn for enzyme **Lactate dehydrogenase (LDH) cytotoxicity assay** analysis (*Lactate Dehydrogenase LDH UV kit*; Bioclin), an assay based on the release of LDH in the culture supernatant.

5.14. Pre-incubation of trypomastigote forms with compound 12

Trypomastigotes forms (1×10^6 cells/mL) were pre-incubated with **12** at 3.125 μM concentration in RPMIc medium for 1 h at 37 °C, 5% CO_2. After incubation the solution was centrifuged at 2438×*g* for 10 min, the supernatant removed and the pellet resuspended in 1 mL of RPMIc for recounting and subsequent infection of the plated macrophages.

5.15. Count of trypomastigote forms

The growth of the parasites was quantified by the number of trypomastigote forms released in the supernatants from 3 days after infection until day 11. 10 μL of the supernatant from the infected wells stimulated or not was collected, placed in the Neubauer chamber and the number of trypomastigote forms counted.

5.16. Nitric oxide detection

Nitric oxide levels were determined (Griess method) in the supernatants harvested at 11 days after infection and/or stimulation of macrophage culture. The nitrite concentration was analyzed by adding 50 μL of the culture supernatant to 0.1 mL of the Griess reagent. After 10 min of reaction, the absorbance at 540 nm was read and the NO_2 concentration was determined.

Ethics statement

This research study was carried out in strict accordance with the Brazilian Guidelines on animal work and the Guide for the Care and Use of Laboratory Animals of the National Institutes of Health (NIH). The animal ethics committee (CEUA) of the Universidade Federal de Minas Gerais (UFMG) approved all experiments and procedures including euthanasia, fluid and organ removal (Permit Number: 89/2010 and 305/2016). All animal experiments were planned in order to minimize mouse suffering.

Funding sources

RSF acknowledges the Brazilian funding agencies Conselho Nacional de Desenvolvimento Científico e Tecnológico (CNPq), Coordenação de Aperfeiçoamento do Ensino Superior (CAPES, Edital Biocomputacional AUXPE 3379/2013), and Fundação de Amparo a Pesquisa do Estado de Minas Gerais (FAPEMIG), L'Oréal-UNESCO-ABC "For Women in Science Award, Category Chemistry, Brazil, 2017" and L'Oréal-UNESCO "For Women in Science International Rising Talents 2018 Award". GANP, RPV and SFB acknowledge postdoctoral fellowships from CAPES (Edital PVE A118/2013 and Edital Biocomputacional AUXPE 3379/2013). RSF, ROB and FSM hold CNPq research fellowships (Bolsa de Produtividade em Pesquisa). Whole-organism screens with *T. brucei* were supported by the US National Institute Of Allergy And Infectious Diseases of the National Institutes of Health under Award Number R21AI133394. The content is solely the responsibility of the authors and does not necessarily represent the official views of the National Institutes of Health. The authors also declare no competing financial interest.

Acknowledgments

We thank the Medicines for Malaria Venture for providing, free of charge, the Malaria box compound set. We also thank the Center of Flow Cytometry and Fluorimetry at the Biochemistry and Immunology Department (UFMG), for access to the fluorimeter, and the Centro de Pesquisas René Rachou (FIOCRUZ) for performing

the UHPLC-HRMS analysis.

Appendix A. Supplementary data

Supplementary data to this article can be found online at https://doi.org/10.1016/j.ejmech.2019.06.062.

Abbreviations

HAT	Human African trypanosomiasis
MMV	Medicines for Malaria Venture
DNDi	Drugs for Neglected Diseases initiative
NTD	neglected tropical diseases
GSK	GlaxoSmithKline
MMV400	Malaria box
μ	micro
Å	angstrom(s)
°C	degrees Celsius
eq	equation
h	hours
IC_{50}	half-maximum inhibitory concentration
Ki	inhibition constant
K_m	Michaelis constant
M	molar
mL	milliliter
mM	millimolar
nm	nanometer(s)
nM	nanomolar
PDB	Protein Data Bank
qHTS	quantitative High-throughput screening qHTS
rpm	revolutions per minute
CHAPS	(3-((3-cholamidopropyl) dimethylammonio)-1-propanesulfonate)
DMSO	dimethylsulfoxide;
EDTA	ethylenediaminetetraacetic acid
Z-VVR-AMC	CBZ-Val-Val-Arg-7-amino-4- methylcoumarin
Z-FR-AMC	CBZ-Phe-Arg-amidomethylcoumarin
LLCMK2	*Macaca mulatta* fibroblast cells line;
RPMI	*Roswell Park Memorial Institute* 1640 medium
RPMIc	RPMI supplemented with 5% fetal bovine serum, 1% L-glutamine, 1% penicillin and 1% streptomycin
MO	macrophages

References

[1] WHO, Chagas disease (American trypanosomiasis), 2017. http://www.who.int/mediacentre/factsheets/fs340/en/, 2017.

[2] WHO, Trypanosomiasis, human African (sleeping sickness), 2017. http://www.who.int/mediacentre/factsheets/fs259/en/, 2017.

[3] WHO, Schistosomiasis, 2017. http://www.who.int/mediacentre/factsheets/fs115/en/, 2017.

[4] WHO, P. Holmes, Investing to Overcome the Global Impact of Neglected Tropical Diseases: Third WHO Report on Neglected Tropical Diseases, Department of control of neglected tropical diseases. World Health Organization, 2015.

[5] M. Garza, T.P. Feria Arroyo, E.A. Casillas, V. Sanchez-Cordero, C.L. Rivaldi, S. Sarkar, Projected future distributions of vectors of Trypanosoma cruzi in North America under climate change scenarios, PLoS Neglected Trop. Dis. 8 (2014), e2818, https://doi.org/10.1371/journal.pntd.0002818.

[6] J.A. Patz, T.K. Graczyk, N. Geller, A.Y. Vittor, Effects of environmental change on emerging parasitic diseases, Int. J. Parasitol. 30 (2000) 1395–1405. http://www.ncbi.nlm.nih.gov/pubmed/11113264.

[7] MMV, Medicines for Malaria Venture, Open access malaria box, 2016, 2016. https://www.mmv.org/research-development/open-source-research/open-access-malaria-box.

[8] T. Spangenberg, J.N. Burrows, P. Kowalczyk, S. McDonald, T.N. Wells, P. Willis, The open access malaria box: a drug discovery catalyst for neglected diseases, PLoS One 8 (2013), e62906, https://doi.org/10.1371/journal.pone.0062906.

[9] I. Pena, M. Pilar Manzano, J. Cantizani, A. Kessler, J. Alonso-Padilla, A.I. Bardera, E. Alvarez, G. Colmenarejo, I. Cotillo, I. Roquero, F. de Dios-Anton, V. Barroso, A. Rodriguez, D.W. Gray, M. Navarro, V. Kumar, A. Sherstnev, D.H. Drewry, J.R. Brown, J.M. Fiandor, J. Julio Martin, New compound sets identified from high throughput phenotypic screening against three kinetoplastid parasites: an open resource, Sci. Rep. 5 (2015) 8771, https://doi.org/10.1038/srep08771.

[10] K. Ingram-Sieber, N. Cowan, G. Panic, M. Vargas, N.R. Mansour, Q.D. Bickle, T.N. Wells, T. Spangenberg, J. Keiser, Orally active antischistosomal early leads identified from the open access malaria box, PLoS Neglected Trop. Dis. 8 (2014), e2610, https://doi.org/10.1371/journal.pntd.0002610.

[11] M. Kaiser, L. Maes, L.P. Tadoori, T. Spangenberg, J.R. Ioset, Repurposing of the open access malaria box for kinetoplastid diseases identifies novel active scaffolds against trypanosomatids, J. Biomol. Screen 20 (2015) 634–645, https://doi.org/10.1177/1087057115569155.

[12] T. Jefferson, D. McShan, J. Warfield, I.V. Ogungbe, Screening and identification of inhibitors of trypanosoma brucei cathepsin L with antitrypanosomal activity, Chem. Biol. Drug Des. 87 (2016) 154–158, https://doi.org/10.1111/cbdd.12628.

[13] M. Khraiwesh, S. Leed, N. Roncal, J. Johnson, R. Sciotti, P. Smith, L. Read, R. Paris, T. Hudson, M. Hickman, M. Grogl, Antileishmanial activity of compounds derived from the Medicines for malaria venture open access box Against intracellular leishmania major amastigotes, Am. J. Trop. Med. Hyg. 94 (2016) 340–347, https://doi.org/10.4269/ajtmh.15-0448.

[14] W.C. Van Voorhis, J.H. Adams, R. Adelfio, V. Ahyong, M.H. Akabas, P. Alano, A. Alday, Y. Aleman Resto, A. Alsibaee, A. Alzualde, K.T. Andrews, S. V Avery, V.M. Avery, L. Ayong, M. Baker, S. Baker, C. Ben Mamoun, S. Bhatia, Q. Bickle, L. Bounaadja, T. Bowling, J. Bosch, L.E. Boucher, F.F. Boyom, J. Brea, M. Brennan, A. Burton, C.R. Caffrey, G. Camarda, M. Carrasquilla, D. Carter, M. Belen Cassera, K. Chih-Chien Cheng, W. Chindaudomsate, A. Chubb, B.L. Colon, D.D. Colon-Lopez, Y. Corbett, G.J. Crowther, N. Cowan, S. D'Alessandro, N. Le Dang, M. Delves, J.L. DeRisi, A.Y. Du, S. Duffy, S. Abd El-Salam El-Sayed, M.T. Ferdig, J.A. Fernandez Robledo, D.A. Fidock, I. Florent, P. V Fokou, A. Galstian, F.J. Gamo, S. Gokool, B. Gold, T. Golub, G.M. Goldgof, R. Guha, W.A. Guiguemde, N. Gural, R.K. Guy, M.A. Hansen, K.K. Hanson, A. Hemphill, R. Hooft van Huijsduijnen, T. Horii, P. Horrocks, T.B. Hughes, C. Huston, I. Igarashi, K. Ingram-Sieber, M.A. Itoe, A. Jadhav, A. Naranuntarat Jensen, L.T. Jensen, R.H. Jiang, A. Kaiser, J. Keiser, T. Ketas, S. Kicka, S. Kim, K. Kirk, V.P. Kumar, D.E. Kyle, M.J. Lafuente, S. Landfear, N. Lee, S. Lee, A.M. Lehane, F. Li, D. Little, L. Liu, M. Llinas, M.I. Loza, A. Lubar, L. Lucantoni, I. Lucet, L. Maes, D. Mancama, N.R. Mansour, S. March, S. McGowan, I. Medina Vera, S. Meister, L. Mercer, J. Mestres, A.N. Mfopa, R.N. Misra, S. Moon, J.P. Moore, F. Morais Rodrigues da Costa, J. Muller, A. Muriana, S. Nakazawa Hewitt, B. Nare, C. Nathan, N. Narraidoo, S. Nawaratna, K.K. Ojo, D. Ortiz, G. Panic, G. Papadatos, S. Parapini, K. Patra, N. Pham, S. Prats, D.M. Plouffe, S.A. Poulsen, A. Pradhan, C. Quevedo, R.J. Quinn, C.A. Rice, M. Abdo Rizk, A. Ruecker, R. St Onge, R. Salgado Ferreira, J. Samra, N.G. Robinett, U. Schlecht, M. Schmitt, F. Silva Villela, F. Silvestrini, R. Sinden, D.A. Smith, T. Soldati, A. Spitzmuller, S.M. Stamm, D.J. Sullivan, W. Sullivan, S. Suresh, B.M. Suzuki, Y. Suzuki, S.J. Swamidass, D. Taramelli, L.R. Tchokouaha, A. Theron, D. Thomas, K.F. Tonissen, S. Townson, A.K. Tripathi, V. Trofimov, K.O. Udenze, I. Ullah, C. Vallieres, E. Vigil, J.M. Vinetz, P. Voong Vinh, H. Vu, N.A. Watanabe, K. Weatherby, P.M. White, A.F. Wilks, E.A. Winzeler, E. Wojcik, M. Wree, W. Wu, N. Yokoyama, P.H. Zollo, N. Abla, B. Blasco, J. Burrows, B. Laleu, D. Leroy, T. Spangenberg, T. Wells, P.A. Willis, Open source drug discovery with the malaria box compound collection for neglected diseases and beyond, PLoS Pathog. 12 (2016), https://doi.org/10.1371/journal.ppat.1005763 e1005763.

[15] M.H. Abdulla, K.C. Lim, M. Sajid, J.H. McKerrow, C.R. Caffrey, Schistosomiasis mansoni: novel chemotherapy using a cysteine protease inhibitor, PLoS Med. 4 (2007) e14, https://doi.org/10.1371/journal.pmed.0040014.

[16] M.H. Abdulla, T. O'Brien, Z.B. Mackey, M. Sajid, D.J. Grab, J.H. McKerrow, RNA interference of Trypanosoma brucei cathepsin B and L affects disease progression in a mouse model, PLoS Neglected Trop. Dis. 2 (2008) e298, https://doi.org/10.1371/journal.pntd.0000298.

[17] P.S. Doyle, Y.M. Zhou, J.C. Engel, J.H. McKerrow, A cysteine protease inhibitor cures Chagas' disease in an immunodeficient-mouse model of infection, Antimicrob. Agents Chemother. 51 (2007) 3932–3939, https://doi.org/10.1128/AAC.00436-07.

[18] J.C. Engel, P.S. Doyle, I. Hsieh, J.H. McKerrow, Cysteine protease inhibitors cure an experimental Trypanosoma cruzi infection, J. Exp. Med. 188 (1998) 725–734. http://www.ncbi.nlm.nih.gov/pubmed/9705954.

[19] E.B. da Silva, G.A. do Nascimento Pereira, R.S. Ferreira, Trypanosomal cysteine peptidases: target validation and drug design strategies, in: Compr. Anal. Parasite Biol. From Metab. To Drug Discov, Wiley-VCH Verlag GmbH & Co. KGaA, 2016, pp. 121–145, https://doi.org/10.1002/9783527694082.ch5.

[20] D. Steverding, D.W. Sexton, X. Wang, S.S. Gehrke, G.K. Wagner, C.R. Caffrey, Trypanosoma brucei: chemical evidence that cathepsin L is essential for survival and a relevant drug target, Int. J. Parasitol. 42 (2012) 481–488, https://doi.org/10.1016/j.ijpara.2012.03.009.

[21] A. Latorre, T. Schirmeister, J. Kesselring, S. Jung, P. Johe, U.A. Hellmich, A. Heilos, B. Engels, R.L. Krauth-Siegel, N. Dirdjaja, L. Bou-Iserte, S. Rodriguez, F. V Gonzalez, Dipeptidyl nitroalkenes as potent reversible inhibitors of cysteine proteases rhodesain and cruzain, ACS Med. Chem. Lett. 7 (2016) 1073–1076, https://doi.org/10.1021/acsmedchemlett.6b00276.

[22] D.C. Greenbaum, Z. Mackey, E. Hansell, P. Doyle, J. Gut, C.R. Caffrey, J. Lehrman, P.J. Rosenthal, J.H. McKerrow, K. Chibale, Synthesis and structure-activity relationships of parasiticidal thiosemicarbazone cysteine protease inhibitors against Plasmodium falciparum, Trypanosoma brucei, and Trypanosoma cruzi,

J. Med. Chem. 47 (2004) 3212–3219, https://doi.org/10.1021/jm030549j.
[23] S.F. Braga, L.C. Martins, E.B. da Silva, P.A. Sales Junior, S.M. Murta, A.J. Romanha, W.T. Soh, H. Brandstetter, R.S. Ferreira, R.B. de Oliveira, Synthesis and biological evaluation of potential inhibitors of the cysteine proteases cruzain and rhodesain designed by molecular simplification, Bioorg. Med. Chem. 25 (2017) 1889–1900, https://doi.org/10.1016/j.bmc.2017.02.009.
[24] K. Brak, I.D. Kerr, K.T. Barrett, N. Fuchi, M. Debnath, K. Ang, J.C. Engel, J.H. McKerrow, P.S. Doyle, L.S. Brinen, J.A. Ellman, Nonpeptidic tetrafluorophenoxymethyl ketone cruzain inhibitors as promising new leads for Chagas disease chemotherapy, J. Med. Chem. 53 (2010) 1763–1773, https://doi.org/10.1021/jm901633v.
[25] C. Bryant, I.D. Kerr, M. Debnath, K.K. Ang, J. Ratnam, R.S. Ferreira, P. Jaishankar, D. Zhao, M.R. Arkin, J.H. McKerrow, L.S. Brinen, A.R. Renslo, Novel nonpeptidic vinylsulfones targeting the S2 and S3 subsites of parasite cysteine proteases, Bioorg. Med. Chem. Lett 19 (2009) 6218–6221, https://doi.org/10.1016/j.bmcl.2009.08.098.
[26] J.P. Mallari, W.A. Guiguemde, R.K. Guy, Antimalarial activity of thiosemicarbazones and purine derived nitriles, Bioorg. Med. Chem. Lett 19 (2009) 3546–3549, https://doi.org/10.1016/j.bmcl.2009.04.142.
[27] S. Previti, R. Ettari, S. Cosconati, G. Amendola, K. Chouchene, A. Wagner, U.A. Hellmich, K. Ulrich, R.L. Krauth-Siegel, P.R. Wich, I. Schmid, T. Schirmeister, J. Gut, P.J. Rosenthal, S. Grasso, M. Zappala, Development of novel peptide-based michael acceptors targeting rhodesain and falcipain-2 for the treatment of neglected tropical diseases (NTDs), J. Med. Chem. 60 (2017) 6911–6923, https://doi.org/10.1021/acs.jmedchem.7b00405.
[28] L.G. Ferreira, A.D. Andricopulo, Targeting cysteine proteases in trypanosomatid disease drug discovery, Pharmacol. Ther. 180 (2017) 49–61, https://doi.org/10.1016/j.pharmthera.2017.06.004.
[29] R.S. Ferreira, A. Simeonov, A. Jadhav, O. Eidam, B.T. Mott, M.J. Keiser, J.H. McKerrow, D.J. Maloney, J.J. Irwin, B.K. Shoichet, Complementarity between a docking and a high-throughput screen in discovering new cruzain inhibitors, J. Med. Chem. 53 (2010) 4891–4905, https://doi.org/10.1021/jm100488w.
[30] N.C. Fonseca, L.F. da Cruz, F. da Silva Villela, G.A. do Nascimento Pereira, J.L. de Siqueira-Neto, D. Kellar, B.M. Suzuki, D. Ray, T.B. de Souza, R.J. Alves, P.A. Sales Junior, A.J. Romanha, S.M. Murta, J.H. McKerrow, C.R. Caffrey, R.B. de Oliveira, R.S. Ferreira, Synthesis of a sugar-based thiosemicarbazone series and structure-activity relationship versus the parasite cysteine proteases rhodesain, cruzain, and Schistosoma mansoni cathepsin B1, Antimicrob. Agents Chemother. 59 (2015) 2666–2677, https://doi.org/10.1128/AAC.04601-14.
[31] A. Jilkova, P. Rezacova, M. Lepsik, M. Horn, J. Vachova, J. Fanfrlik, J. Brynda, J.H. McKerrow, C.R. Caffrey, M. Mares, Structural basis for inhibition of cathepsin B drug target from the human blood fluke, Schistosoma mansoni, J. Biol. Chem. 286 (2011) 35770–35781, https://doi.org/10.1074/jbc.M111.271304.
[32] H.J. Wiggers, J.R. Rocha, W.B. Fernandes, R. Sesti-Costa, Z.A. Carneiro, J. Cheleski, A.B. da Silva, L. Juliano, M.H. Cezari, J.S. Silva, J.H. McKerrow, C.A. Montanari, Non-peptidic cruzain inhibitors with trypanocidal activity discovered by virtual screening and in vitro assay, PLoS Neglected Trop. Dis. 7 (2013), e2370, https://doi.org/10.1371/journal.pntd.0002370.
[33] B.T. Mott, R.S. Ferreira, A. Simeonov, A. Jadhav, K.K. Ang, W. Leister, M. Shen, J.T. Silveira, P.S. Doyle, M.R. Arkin, J.H. McKerrow, J. Inglese, C.P. Austin, C.J. Thomas, B.K. Shoichet, D.J. Maloney, Identification and optimization of inhibitors of Trypanosomal cysteine proteases: cruzain, rhodesain, and TbCatB, J. Med. Chem. 53 (2010) 52–60, https://doi.org/10.1021/jm901069a.
[34] R.S. Ferreira, M.A. Dessoy, I. Pauli, M.L. Souza, R. Krogh, A.I. Sales, G. Oliva, L.C. Dias, A.D. Andricopulo, Synthesis, biological evaluation, and structure-activity relationships of potent noncovalent and nonpeptidic cruzain inhibitors as anti-Trypanosoma cruzi agents, J. Med. Chem. 57 (2014) 2380–2392, https://doi.org/10.1021/jm401709b.
[35] R.P. Vieira, V.C. Santos, R.S. Ferreira, Structure-based approaches targeting parasite cysteine proteases, Curr. Med. Chem. (2017), https://doi.org/10.2174/0929867324666170810165302.
[36] J.W. Espindola, M. V Cardoso, G.B. Filho, E.S.D.A. Oliveira, D.R. Moreira, T.M. Bastos, C.A. Simone, M.B. Soares, F.S. Villela, R.S. Ferreira, M.C. Castro, V.R. Pereira, S.M. Murta, P.A. Sales Junior, A.J. Romanha, A.C. Leite, Synthesis and structure-activity relationship study of a new series of antiparasitic aryloxyl thiosemicarbazones inhibiting Trypanosoma cruzi cruzain, Eur. J. Med. Chem. 101 (2015) 818–835, https://doi.org/10.1016/j.ejmech.2015.06.048.
[37] D.A. Rocha, E.B. Silva, I.S. Fortes, M.S. Lopes, R.S. Ferreira, S.F. Andrade, Synthesis and structure-activity relationship studies of cruzain and rhodesain inhibitors, Eur. J. Med. Chem. 157 (2018) 1426–1459, https://doi.org/10.1016/j.ejmech.2018.08.079.
[38] M. Giroud, B. Kuhn, S. Saint-Auret, C. Kuratli, R.E. Martin, F. Schuler, F. Diederich, M. Kaiser, R. Brun, T. Schirmeister, W. Haap, 2 H-1,2,3-Triazole-Based dipeptidyl nitriles: potent, selective, and trypanocidal rhodesain inhibitors by structure-based design, J. Med. Chem. 61 (2018) 3370–3388, https://doi.org/10.1021/acs.jmedchem.7b01870.
[39] X. Du, C. Guo, E. Hansell, P.S. Doyle, C.R. Caffrey, T.P. Holler, J.H. McKerrow, F.E. Cohen, Synthesis and structure-activity relationship study of potent trypanocidal thio semicarbazone inhibitors of the trypanosomal cysteine protease cruzain, J. Med. Chem. 45 (2002) 2695–2707. https://www.ncbi.nlm.nih.gov/pubmed/12061873.
[40] J.P. Mallari, A.A. Shelat, T. Obrien, C.R. Caffrey, A. Kosinski, M. Connelly, M. Harbut, D. Greenbaum, J.H. McKerrow, R.K. Guy, Development of potent purine-derived nitrile inhibitors of the trypanosomal protease TbcatB, J. Med. Chem. 51 (2008) 545–552, https://doi.org/10.1021/jm070760l.
[41] B.Y. Feng, A. Simeonov, A. Jadhav, K. Babaoglu, J. Inglese, B.K. Shoichet, C.P. Austin, A high-throughput screen for aggregation-based inhibition in a large compound library, J. Med. Chem. 50 (2007) 2385–2390, https://doi.org/10.1021/jm061317y.
[42] K. Babaoglu, A. Simeonov, J.J. Irwin, M.E. Nelson, B. Feng, C.J. Thomas, L. Cancian, M.P. Costi, D.A. Maltby, A. Jadhav, J. Inglese, C.P. Austin, B.K. Shoichet, Comprehensive mechanistic analysis of hits from high-throughput and docking screens against beta-lactamase, J. Med. Chem. 51 (2008) 2502–2511, https://doi.org/10.1021/jm701500e.
[43] A. Jadhav, R.S. Ferreira, C. Klumpp, B.T. Mott, C.P. Austin, J. Inglese, C.J. Thomas, D.J. Maloney, B.K. Shoichet, A. Simeonov, Quantitative analyses of aggregation, autofluorescence, and reactivity artifacts in a screen for inhibitors of a thiol protease, J. Med. Chem. 53 (2010) 37–51, https://doi.org/10.1021/jm901070c.
[44] S.L. McGovern, E. Caselli, N. Grigorieff, B.K. Shoichet, A common mechanism underlying promiscuous inhibitors from virtual and high-throughput screening, J. Med. Chem. 45 (2002) 1712–1722. http://www.ncbi.nlm.nih.gov/pubmed/11931626.
[45] B.Y. Feng, B.K. Shoichet, A detergent-based assay for the detection of promiscuous inhibitors, Nat. Protoc. 1 (2006) 550–553, https://doi.org/10.1038/nprot.2006.77.
[46] R.S. Ferreira, C. Bryant, K.K. Ang, J.H. McKerrow, B.K. Shoichet, A.R. Renslo, Divergent modes of enzyme inhibition in a homologous structure-activity series, J. Med. Chem. 52 (2009) 5005–5008, https://doi.org/10.1021/jm9009229.
[47] E.S. Voropai, M.P. Samtsov, K.N. Kaplevskii, A.A. Maskevich, V.I. Stepuro, O.I. Povarova, I.M. Kuznetsova, K.K. Turoverov, A.L. Fink, V.N. Uversky, Spectral properties of Thioflavin T and its complexes with amyloid fibrils, J. Appl. Spectrosc. 70 (2003) 868–874, https://doi.org/10.1023/B:JAPS.0000016303.37573.7e.
[48] S.A. Gillmor, C.S. Craik, R.J. Fletterick, Structural determinants of specificity in the cysteine protease cruzain, Protein Sci. 6 (1997) 1603–1611, https://doi.org/10.1002/pro.5560060801.
[49] I.D. Kerr, P. Wu, R. Marion-Tsukamaki, Z.B. Mackey, L.S. Brinen, Crystal Structures of TbCatB and rhodesain, potential chemotherapeutic targets and major cysteine proteases of Trypanosoma brucei, PLoS Neglected Trop. Dis. 4 (2010), e701, https://doi.org/10.1371/journal.pntd.0000701.
[50] Schrödinger Release 2015-3: Schrödinger Suite 2015-3 Induced Fit Docking Protocol; Glide, Schrödinger, LLC, New York, NY, 2016; Prime, Schrödinger, LLC, New York, NY, 2015, p. 2015.
[51] I.D. Kerr, J.H. Lee, C.J. Farady, R. Marion, M. Rickert, M. Sajid, K.C. Pandey, C.R. Caffrey, J. Legac, E. Hansell, J.H. McKerrow, C.S. Craik, P.J. Rosenthal, L.S. Brinen, Vinyl sulfones as antiparasitic agents and a structural basis for drug design, J. Biol. Chem. 284 (2009) 25697–25703, https://doi.org/10.1074/jbc.M109.014340.
[52] R.A. Martinez-Diaz, J.A. Escario, J.J. Nogal-Ruiz, A. Gomez-Barrio, Biological characterization of Trypanosoma cruzi strains, Mem. Inst. Oswaldo Cruz 96 (2001) 53–59. https://www.ncbi.nlm.nih.gov/pubmed/11285475.
[53] A.F. Abdel-Magid, K.G. Carson, B.D. Harris, C.A. Maryanoff, R.D. Shah, Reductive amination of aldehydes and ketones with sodium triacetoxyborohydride. Studies on direct and indirect reductive amination procedures(1), J. Org. Chem. 61 (1996) 3849–3862. https://www.ncbi.nlm.nih.gov/pubmed/11667239.
[54] R.B. Oliveira, C.L. Zani, R.S. Ferreira, R.S. Leite, T.M. Alves, T.H.A. Silva, A.J. Romanha, Síntese, avaliação biológica e modelagem molecular de arilfuranos como inibidores da enzima tripanotiona redutase, Quim. Nova 31 (2008) 261–267.
[55] E. Salas-Sarduy, L.U. Landaburu, J. Karpiak, K.P. Madauss, J.J. Cazzulo, F. Aguero, V.E. Alvarez, Novel scaffolds for inhibition of Cruzipain identified from high-throughput screening of anti-kinetoplastid chemical boxes, Sci. Rep. 7 (2017) 12073, https://doi.org/10.1038/s41598-017-12170-4.
[56] G.A.N. Pereira, L.H. Santos, S.C. Wang, L.C. Martins, F.S. Villela, W. Liao, M.A. Dessoy, L.C. Dias, A.D. Andricopulo, M.A.F. Costa, R.A.P. Nagem, C.R. Caffrey, K.R. Liedl, E.R. Caffarena, R.S. Ferreira, Benzimidazole inhibitors of the major cysteine protease of Trypanosoma brucei, Future Med. Chem. Accepted (2019), https://doi.org/10.4155/fmc-2018-0523.
[57] L.H. Santos, B.J. Waldner, J.E. Fuchs, G.A.N. Pereira, K.R. Liedl, E.R. Caffarena, R.S. Ferreira, Understanding structure-activity relationships for trypanosomal cysteine protease inhibitors by simulations and free energy calculations, J. Chem. Inf. Model. (2019), https://doi.org/10.1021/acs.jcim.8b00557.
[58] Y. Choe, F. Leonetti, D.C. Greenbaum, F. Lecaille, M. Bogyo, D. Bromme, J.A. Ellman, C.S. Craik, Substrate profiling of cysteine proteases using a combinatorial peptide library identifies functionally unique specificities, J. Biol. Chem. 281 (2006) 12824–12832, https://doi.org/10.1074/jbc.M513331200.
[59] M.E. McGrath, J.T. Palmer, D. Bromme, J.R. Somoza, Crystal structure of human cathepsin S, Protein Sci. 7 (1998) 1294–1302, https://doi.org/10.1002/pro.5560070604.
[60] I.M. Aparicio, J. Scharfstein, A.P. Lima, A new cruzipain-mediated pathway of human cell invasion by Trypanosoma cruzi requires trypomastigote membranes, Infect. Immun. 72 (2004) 5892–5902, https://doi.org/10.1128/IAI.72.10.5892-5902.2004.
[61] A.A. Mielniczki-Pereira, C.M. Chiavegatto, J.A. Lopez, W. Colli, M.J. Alves,

F.R. Gadelha, Trypanosoma cruzi strains, Tulahuen 2 and Y, besides the difference in resistance to oxidative stress, display differential glucose-6-phosphate and 6-phosphogluconate dehydrogenases activities, Acta Trop. 101 (2007) 54–60, https://doi.org/10.1016/j.actatropica.2006.12.001.
[62] C.R. Caffrey, E. Hansell, K.D. Lucas, L.S. Brinen, A. Alvarez Hernandez, J. Cheng, S.L. Gwaltney 2nd, W.R. Roush, Y.D. Stierhof, M. Bogyo, D. Steverding, J.H. McKerrow, Active site mapping, biochemical properties and subcellular localization of rhodesain, the major cysteine protease of Trypanosoma brucei rhodesiense, Mol. Biochem. Parasitol. 118 (2001) 61–73. http://www.ncbi.nlm.nih.gov/pubmed/11704274.
[63] M. Sajid, J.H. McKerrow, E. Hansell, M.A. Mathieu, K.D. Lucas, I. Hsieh, D. Greenbaum, M. Bogyo, J.P. Salter, K.C. Lim, C. Franklin, J.H. Kim, C.R. Caffrey, Functional expression and characterization of Schistosoma mansoni cathepsin B and its trans-activation by an endogenous asparaginyl endopeptidase, Mol. Biochem. Parasitol. 131 (2003) 65–75. http://www.ncbi.nlm.nih.gov/pubmed/12967713.
[64] R. Freier, E. Dall, H. Brandstetter, Protease recognition sites in Bet v 1a are cryptic, explaining its slow processing relevant to its allergenicity, Sci. Rep. 5 (2015) 12707, https://doi.org/10.1038/srep12707.
[65] One-way ANOVA Followed by Dunnett's Multiple Comparisons Test Was Performed Using GraphPad Prism Version 6.00 for Windows, GraphPad Software, La Jolla California, USA (n.d.) www.graphpad.com
[66] X.F. Ren, H.W. Li, X. Fang, Y. Wu, L. Wang, S. Zou, Highly selective azadipeptide nitrile inhibitors for cathepsin K: design, synthesis and activity assays, Org. Biomol. Chem. 11 (2013) 1143–1148, https://doi.org/10.1039/c2ob26624e.
[67] J.C. Krupa, J.S. Mort, Optimization of detergents for the assay of cathepsins B, L, S, and K, Anal. Biochem. 283 (2000) 99–103, https://doi.org/10.1006/abio.2000.4621.
[68] Schrödinger Release 2015-3, Maestro Schrödinger, LLC, New York, NY, 2015 version 10.3, (n.d.).
[69] Schrödinger Release 2015-3, LigPrep Schrödinger, LLC, New York, NY, 2015 version 3.5, (n.d.).
[70] J.R. Greenwood, D. Calkins, A.P. Sullivan, J.C. Shelley, Towards the comprehensive, rapid, and accurate prediction of the favorable tautomeric states of drug-like molecules in aqueous solution, J. Comput. Aided Mol. Des. 24 (2010) 591–604, https://doi.org/10.1007/s10822-010-9349-1.
[71] J.C. Shelley, A. Cholleti, L.L. Frye, J.R. Greenwood, M.R. Timlin, M. Uchimaya, Epik: a software program for pK(a) prediction and protonation state generation for drug-like molecules, J. Comput. Aided Mol. Des. 21 (2007) 681–691, https://doi.org/10.1007/s10822-007-9133-z.
[72] Schrödinger Release 2015-3, Epik Schrödinger, LLC, New York, NY, 2015 version 3.3, (n.d.).
[73] R. Marion, E. Hansell, C.R. Caffrey, W.R. Roush, L.S. Brinen, The High Resolution Crystal Structure of Rohedsain, the Major Cathepsin L Protease from T. Brucei Rhodesiense, Bound to Inhibitor K11002, 2007, https://doi.org/10.2210/pdb2P86/pdb.
[74] Schrödinger Release 2015-3: Schrödinger Suite 2015-3 Protein Preparation Wizard; Epik, Schrödinger, LLC, New York, NY, 2015 Version 3.3; Impact, Schrödinger, LLC, New York, NY, 2015, Version 6.8; Prime, Schrödinger, LLC, New York, NY, 2015 version 4.1, (n.d.).
[75] G.M. Sastry, M. Adzhigirey, T. Day, R. Annabhimoju, W. Sherman, Protein and ligand preparation: parameters, protocols, and influence on virtual screening enrichments, J. Comput. Aided Mol. Des. 27 (2013) 221–234, https://doi.org/10.1007/s10822-013-9644-8.
[76] A.C. Storer, R. Menard, Catalytic mechanism in papain family of cysteine peptidases, Methods Enzymol. 244 (1994) 486–500. http://www.ncbi.nlm.nih.gov/pubmed/7845227.
[77] O. Mendez-Lucio, A. Romo-Mancillas, J.L. Medina-Franco, R. Castillo, Computational study on the inhibition mechanism of cruzain by nitrile-containing molecules, J. Mol. Graph. Model. 35 (2012) 28–35, https://doi.org/10.1016/j.jmgm.2012.01.003.
[78] Small-Molecule Drug Discovery Suite 2015-3, Schrödinger, LLC, New York, NY, 2015 version 6.4, (n.d.).
[79] T.A. Halgren, R.B. Murphy, R.A. Friesner, H.S. Beard, L.L. Frye, W.T. Pollard, J.L. Banks, Glide: a new approach for rapid, accurate docking and scoring. 2. Enrichment factors in database screening, J. Med. Chem. 47 (2004) 1750–1759, https://doi.org/10.1021/jm030644s.
[80] R.A. Friesner, J.L. Banks, R.B. Murphy, T.A. Halgren, J.J. Klicic, D.T. Mainz, M.P. Repasky, E.H. Knoll, M. Shelley, J.K. Perry, D.E. Shaw, P. Francis, P.S. Shenkin, Glide: a new approach for rapid, accurate docking and scoring. 1. Method and assessment of docking accuracy, J. Med. Chem. 47 (2004) 1739–1749, https://doi.org/10.1021/jm0306430.
[81] W. Sherman, T. Day, M.P. Jacobson, R.A. Friesner, R. Farid, Novel procedure for modeling ligand/receptor induced fit effects, J. Med. Chem. 49 (2006) 534–553, https://doi.org/10.1021/jm050540c.
[82] The PyMOL Molecular Graphics System LLC., Version 1.7.0.0 Schrödinger, (n.d.).
[83] T. Liu, Y. Lin, X. Wen, R.N. Jorissen, M.K. Gilson, BindingDB: a web-accessible database of experimentally determined protein-ligand binding affinities, Nucleic Acids Res. 35 (2007) D198–D201, https://doi.org/10.1093/nar/gkl999.
[84] J.L. Durant, B.A. Leland, D.R. Henry, J.G. Nourse, Reoptimization of MDL keys for use in drug discovery, J. Chem. Inf. Comput. Sci. 42 (2002) 1273–1280. http://www.ncbi.nlm.nih.gov/pubmed/12444722.
[85] RDKit, Open-source Cheminformatics, 2015.